Semarak International Journal of
Fundamental and Applied Mathematics

Journal homepage:
https://semarakilmu.my/index.php/sijfam/index
ISSN: 3030-5527

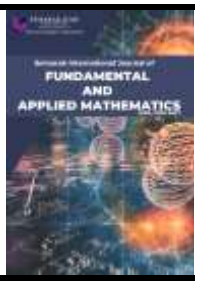

Magneto-Hydrodynamic Scrutiny of Thermal Stratification in a Self-Similar Casson-Walter-B Non-Newtonian Fluid over a Porous Vertical Plate

Ebenezer Olubunmi Ige[1,2,*], Bidemi Olumide Falodun[3], Lukman Olamilekan Ahmed[4]

[1] Department of Mechanical and Mechatronic Engineering, Afe Babalola University Ado-Ekiti – 360231 Nigeria
[2] Department of Biomedical Engineering, Afe Babalola University Ado-Ekiti – 360231 Nigeria
[3] Department of Mathematical and Physical Sciences, Novena University Ogume Nigeria
[4] Department of Mathematica and Physical Sciences Baze University Abuja Nigeria

ARTICLE INFO

Article history:
Received 11 March 2025
Received in revised form 10 April 2025
Accepted 14 May 2025
Available online 30 June 2025

Keywords:
Mass transfer; heat transfer; thermo-hydraulic; thermo-physical properties; spectral homotopy analysis method

ABSTRACT

Thermal stratification of magneto-hydrodynamic self-similar Casson-Walters-B non-Newtonian fluids past a porous vertical plate is explored in this paper. The occurrence of this nature is plausible in industrial processes such as polymer industries. The numerical investigation in this paper is a binary solution which consists of Casson and Walters-B type of fluids. The flow equations that govern the study are nonlinear coupled partial differential equations (PDEs). These sets of PDEs were evaluated using suitable variables to obtain nonlinear ordinary differential equations (ODEs). The set of transformed ODEs were solved numerically by employing the spectral homotopy analysis method (SHAM). SHAM combines the Chebyshev pseudospectral approach with the homotopy analysis method in solving set of differential equations. From the physical point of view, the significance of each pertinent flow parameters is discussed with the help of graphical results. It was found that the plastic dynamic viscosity greatly affects the velocity of Casson fluid within the boundary layer. In the thermally-stratified boundary layer, the magnetic parameter was found to slow down the motion of an electrically conducting fluid due to Lorentz force. The rate of heat transport was determined by pertinent flow parameters such as thermal radiation, viscous dissipation, and heat generation. For example, thermal radiation becomes very significant at a very high temperature, and viscous dissipation in firctional heating of fluid particles. The validation conducted in this paper shows the accuracy of SHAM. The comparison of the present results are previously published works are in good agreement.

1. Introduction

Thermal stratification is a phenomenon that occurs at the interface of two fluids with similar thermo-physical properties in which thermal buoyancy drives the formation of the distinct strata-wise settlement of the fluid within confinement [1]. This is a natural occurrence in static water bodies when the warm surface layer of water has been exposed the sunlight becomes less dense than the underneath strata of cold water which is pronounced in the lower column of the water body. Once

* *Corresponding author.*
E-mail address: author.mail@gmail.com

https://doi.org/10.37934/sijfam.6.1.4166

established, stratification prevails temperature until a session of failing temperature returns in the vicinity of the confinement. The subject of thermal stratification is significant to the study of process engineering because of many natural occurrences. The assessment of thermal stratification in coastal bodies is crucial in the management of aquatic bodies. This is important because a rapid change in pond stratification could threaten the survival of water bodies. Furthermore, the phenomenon of thermal stratification in solar energy concern has informed the concept of stratified thermal energy storage systems in harvesting of renewable solar energy [2-4].

The emerging applications in thermal stratification have curried the interest of researchers in recent years. Hayat [5] explored the thermo-reactive Cattaneo-Christov theory to describe the impact of flow stagnation on the dynamic of thermal stratification for Jerry-type fluid in the vicinity of cylindrically-stretched confinement. In a similar report, Nadeem and Mohammad [6] utilized the Cattaneo-Christov model to analyze thermal conduction using credible transformation schemes to show that a selected relaxation parameter is required in the thermal field to sufficiently illustrate thermal stratification in a porous media. [7] utilized the Drift-Flux model (DFM) which followed a multiplexed Eulerian and discrete phase approach to numerically describe stratification in momentum and thermal field in an attempt to capture particulate matter in a dusty fluid. [8] revealed the occurrence of double stratification in thermal and concentration fields in a Jeffrey-type nanofluid for which the influences of skin friction on the dynamics of stratified is sufficiently elucidated. [9] illustrated the diminishing role of thermal stratification on the temperature field in addition to the incidence of solutal stratification and decay on concentration parameters. [10] analyzed thermal stratification in atmospheric fluids using scaling laws over-described wavelength and climatic changes within the scope of the numerical study. [11] addressed double stratification with chemical reaction and combined exposure of thermal radiation and ohmic heating such that the stratification was observed dominance in the concentration field for consumption in the magnitude of reference nanoparticle embedded within the fluidic media. [12] numerically established the effect of stratification phenomenon in Darcy-Forchheimer flow through the needle-like aperture.

The imposition of externally imposed field effects could trigger the emergence of thermal stratification in fluid media within the vicinity of the fluid media, this field-mediated stratification may be explored for specialized applications of industrial concerns such as thermal storage devices [13,14]. [15,16] showed the decay of momentum field for increasing magnitude of combined magnetic field and suction in a stratified flow with carbon nanotube type nanofluid subjected to bioconvection with an externally-imposed magnetic field. [17] reported the contribution of thermal stratification on the development of boundary layers in cylindrical confinement based on mixed convective and stratification parameters. [18] reported the interrelationship between temperature and thermal stratification parameters under homogenous and heterogeneous consideration which revealed that temperature is decreased due to thermal stratification. The converse behavior is obtainable for the concentration field. [19] analyzed thermal convection in Jerry-type nanofluid which is undergoing the effect of stratification induced by an externally-imposed magnetic field. Their report categorically elucidates the contribution of heat absorption and thermal radiation to the magneto-hydrodynamic flow problem. [20] revealed that the rate of thermal transport in Cu-Al2O33-water hybrid nanofluid is impeded by thermal stratification which is made pronounced by the incidence of thermal buoyancy in the nano liquid for the duo of stretching and shrinking scenarios. A similar observation by Rehman and co-workers narrated the magnitude decay of fluid parameters over the thermal conductivity index which translates to the breakdown of stratification dominance in the thermal field [21]. Hayat and fellow numerically investigated the consequence of double thermal stratification on the occurrence of stretching and shrinking over magnetically conducting second-class nano liquid subjected to heat generation and suction [22].

It has been deemed impractical to examine fluid motion with constant viscosity and thermal conductivity. This is because, as fluids move, their viscosity changes with thermal conductivity due to particle collisions, resulting in cohesive force. As a result, numerous authors have recently focused on the motion of liquids by altering viscosity and thermal conductivity. Khan and colleagues [23] looked at how viscosity and thermal conductivity varied in a thin film flow. [24] investigate the effects of changing viscosity and thermal conductivity on free convective heat and mass transport in non-Newtonian Casson fluid flow. In an angled magnetic field, [25] looked at the effects of varying viscosity and thermal conductivity. [26] looked at the effects of changing thermal conductivity and viscosity on Casson nanofluid flow. The utility of non-Newtonian fluid in food processing, crude oil extraction from petroleum, and chemical engineering drew the attention of many researchers. In high-polymer additives for improving flow in petroleum pipelines, this sort of fluid is highly useful. The flow properties of WaltersB liquid fluid were investigated in [27]. Mishra and colleagues [28] investigated heat and mass transmission in an MHD Walters B nanofluid flow. The flow of Walters B fluid with a convective boundary condition was studied in [29]. [30] investigated viscoelastic fluid boundary layer flow past a nonlinearly stretching sheet. [31] reported the impact of magnetic field on the uniformly applied magnetic field on coupled Eyring-Powell type nonnewtonian fluid. [32] investigated viscoelastic fluid flow in a stretched cylinder with mixed convection. [33] identified the dependence of momentum cum Darcy parameters on suction and injection in a porous on the strength of scaling lie group numerical scheme. [34] investigated Walters B viscoelastic MHD flow in a vertical porous plate that was unstable. [35] investigated a porous media with an unstable MHD non-Newtonian Walter's B fluid. Many researchers have recently become interested in the Casson non-Newtonian fluid.

When the shear stress is smaller than the yield stress, the Casson fluid model seems solid. It also deforms when the shear stress exceeds the yield stress. This is how the blood behaves. [36] investigated Casson fluid flow through a stretching cylinder. [37] investigated Casson fluid heat transfer in non-Darcy porous media. [38] looked at Casson nanofluid flow in three dimensions over a stretching sheet. When a conductor moves into a magnetic field regularly, MHD is studied. The movements of some conductor fluids are complicated. In addition, currents are created in a moment by the motion of an electrically conducting fluid due to the magnetic field, which causes the Lorentz force to decelerate the fluid's speed. Metal cooling, power generators, MHD accelerators, and other applications rely heavily on MHD. [39] investigated heat and mass transfer in MHD Casson fluid as a result of these uses. [40] explain Casson fluid flow with unstable hydrodynamics. [41] investigated MHD micropolar fluid mixed convection flow. MHD flow and heat transmission across a porous shrinking surface was discussed in [42]. [43] investigated the effect of melting on MHD Casson fluid flow lately. MHD boundary-layer flow and melting heat transfer of Williamson nanofluid in the porous medium were investigated by Krishnamurthy and colleagues [44]. MHD flow of Williamson fluid with slippage was discussed by Lund and colleagues [45]. Salawu and Dada [46] investigated the effects of thermal conductivity and varying viscosity on radiative heat transfer in an inclined magnetic field. To the best of the author's knowledge, the impact of variable viscosity and thermal conductivity distribution on the formation of stratified layers of non-Newtonian fluids in the context of thermal stratification in nanoliquid media has not been addressed in the literature. [47] recently did investigation on effects of varying geometrical configurations on thermal hydraulics flow. [48] studied flow field and heat transfer enhancement by using combined corrugated tubes with a twisted tape within 3D circular tube based on different dimple configurations. A numerical study to investigate the effect of turbalators on thermal flow and heat performance of a 3D pipe was investigated by [49]. The recent study of [50] examined thermal flow and heat performance analyses in circular pipe by using distinct twisted tape parameters based in design of experiments. In 2021,

investigation of flow pattern, thermohydraulic performance and improvement of heat transfer in 3D corrugated circular pipe was considered by [51]. In another study of [52], the effect of distinct twisted tape inserts configurations on fluid flow characteristics, pressure drop, thermo-hydraulic performance and heat transfer enhancement was considered. Characterization of internal thermohydraulic flow and heat transfer improvement in a three-dimensional circular corrugated tube surfaces using numerical simulation and experiment design was considered by [53].

The present numerical experiment is designed to examine the contribution of thermal stratification in the formation of viscosity disparity between adjacent layers of nano liquid media in the vicinity of externally-imposed magnetic. A study of this type has not been considered in literature to the best of our knowledge. The study of [54] only examined the flow of Casson fluid in an accelerating medium. A special focus on Casson-WalterB type nanofluid is considered based on the suitability of its rheology to environment-prone hot water. This study initiates thermal stratification by utilizing electromagnetic heating occasioned by an externally-imposed magnetic field in the Casson-Walter non-Newtonian fluid. We provide an elaborate numerical description and statistical analysis of the patterning of variability in the viscosity of the fluid using the elegant Spectra homotopy analysis method, and linear and quadratic multiple regression analysis. Leveraging on the Chebyshev type convergence scheme, the numerical computation was pursued selected environment-informed scenarios of thermal stratification in the attempt to elucidate engineering curiosity on the profiling of skin friction amongst other parameters. The statistical analysis was conducted on the quantities of engineering interest through bar chats.

2. Heat Transfer Analysis

Consider the laminar, steady, viscous, and incompressible motion of Casson together with Walters-B liquid through a porous vertical late into the boundary layer domain. The liquid is considered to be electrically conducting as a magnetism of constant strength is imposed towards the flow direction. The physical geometry as depicted in Figure 1 explains the motion of Casson together with Walters-B liquid into the layers from the penetrable upward plate. The liquids are both set into motion with altered viscosity along with thermal conductivity. The x-axis is examined towards the upward coordinate while the y-coordinate is normal to it (see Figure 1). As seen in Figure 1, the ambient environment is assumed to be hot and thermally stratified. To further explored the process of heat transport, the following assumptions are considered:

i) Assuming magnetic Reynolds number to be very small in such away induced magnetism is ignored;
ii) The wall concentration and temperature are C_w and T_w respectively;
iii) The temperature as well as concentration at the ambient environment are T_∞ and C_∞ respectively;
iv) The vertical plate is surmised to be cool such that $Tw < T_\infty$ and $C_w < C_\infty$;
v) The body force due to non-uniform temperature is $g\beta_t(T - T_\infty)$;
vi) The radiative temperature flux in x-direction is neglected compared to y-direction;
vii) The viscous dissipative and Darcy law is considered at constant penetrable medium;
viii) (viii)The physical liquid properties like viscosity alongwith thermal conductivity are considered to vary within the boundary layer;
ix) A case whereby the vicinity far from the plate is thermally stratified and hot is considered.

Considering the analysis in [55] and the assumptions above the governing equations becomes:

$$\frac{\partial u}{\partial x}+\frac{\partial v}{\partial y}=0 \tag{1}$$

$$u\frac{\partial u}{\partial x}+v\frac{\partial u}{\partial y}=\frac{\partial \tau_{xx}}{\partial x}+\frac{\partial \tau_{xy}}{\partial y}+g\beta_t(T-T_\infty)-\frac{\sigma B_0^2}{\rho}u-\frac{\mu_0}{K}u \tag{2}$$

$$u\frac{\partial T}{\partial x}+v\frac{\partial T}{\partial y}=\frac{k(T)}{\rho c_p}\frac{\partial^2 T}{\partial y^2}+\frac{1}{\rho c_p}\frac{\partial T}{\partial y}\frac{\partial k(T)}{\partial y}-\frac{1}{\rho c_p}\frac{\partial q_r}{\partial y}+\frac{\mu_0}{c_p}\left(\frac{\partial u}{\partial y}\right)^2-\frac{Q_0}{\rho c_p}(T-T_\infty) \tag{3}$$

subject to the boundary constraints

$$u=Bx \quad ,v=-v(x) \ ,T=T_w at \quad y=0 \tag{4}$$

$$u\longrightarrow 0 \quad ,T\longrightarrow T_\infty as \quad y\longrightarrow\infty \tag{5}$$

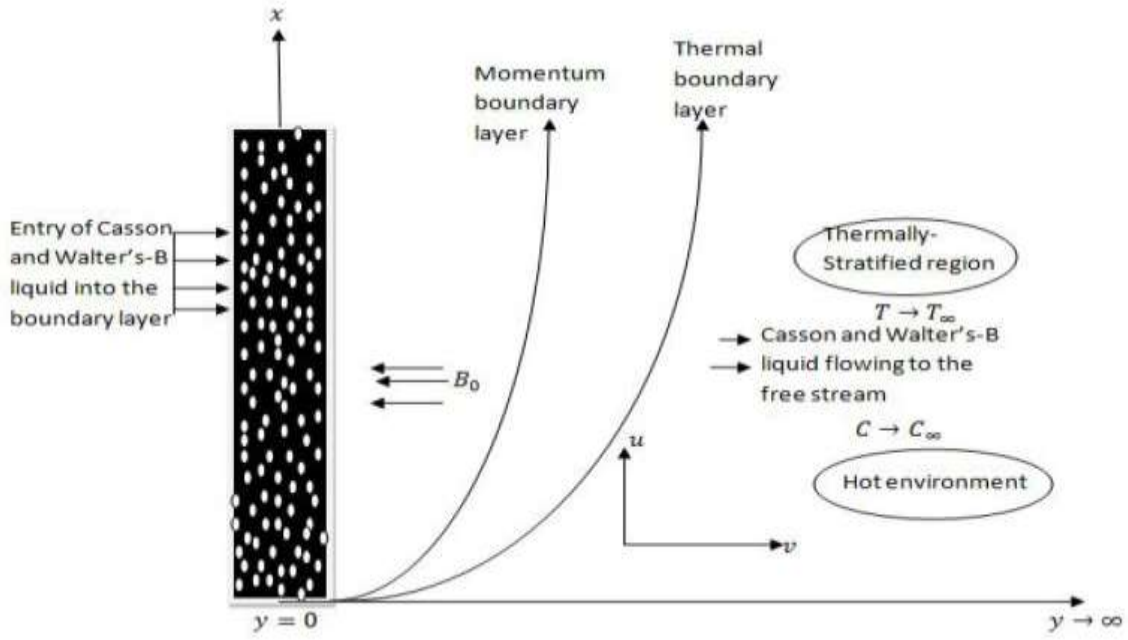

Fig. 1. Flow geometry

This paper considered the model of Casson together with Walters-B liquid. Base on Fredrickson [23] and viscosity definition $\left(\tau=\mu\frac{\partial u}{\partial y}|_{y=0}\right)$, the rheological flow equations of Casson liquid are as follows:

$$\tau_{ij}=\left(\mu_b+\frac{P_y}{\sqrt{2\pi}}\right)2e_{ij} \quad when \quad \pi>\pi_c \tag{6}$$
$$\tau_{ij}=\left(\mu_b+\frac{P_y}{\sqrt{2\pi_c}}\right)2e_{ij} \quad when \quad \pi<\pi_c$$

The fluid yield stress in (6) is P_y and it is given as:

$$P_y=\frac{\mu_b\sqrt{(2\pi)}}{\beta} \tag{7}$$

Note that $\pi = e_{ij}e_{ij}$ mean component of deformation rate multiplying itself and μ_b signifies Casson liquid plastic dynamic viscosity, π_c signifies critical value of Casson liquid model. It worth noting that the Casson liquid plastic dynamic viscosity is varied and when $\pi > \pi_c$ we have that:

$$\mu_0 = \mu_b + \frac{P_y}{\sqrt{2\pi}} \tag{8}$$

Now, substituting Eq. (7) into Eq. (8), it is expedient to say that kinematic viscosity is dependent of the variable plastic dynamic viscosity μ_b. With the above simplifications and assumptions, the Casson fluid parameter results to

$$\mu_0 = \frac{\mu_b}{\rho}\left(1 + \frac{1}{\beta}\right) \tag{9}$$

Note that ρ signifies liquid density and in the study of Mehmood et al.[47], Walters-B liquid fluid Cauchy stress tensor S is given as:

$$S = -pT + \tau \tag{10}$$

$$\tau = 2\eta_0 e - 2k_0 \frac{\delta e}{\delta t} \tag{11}$$

The rate of strain tensor e is given as:

$$2e = \nabla(v) + \nabla(v)^T \tag{12}$$

$\frac{\delta}{\delta t}$ signifies tensor quantity convected differentiation subject to the moving material. It gives

$$\frac{\delta e}{\delta t} = \frac{\partial e}{\partial t} + v.\nabla(e) - e.\nabla(v) - (\nabla(v))^T.e \tag{13}$$

k_0 signifies coefficient of Walters-B memory and it is given as:

$$\eta_0 = \int_0^\infty \lambda(\xi)d\xi \tag{14}$$

$$k_0 = \int_0^\infty \tau\lambda(\xi)d\xi \tag{15}$$

$\lambda(\xi)$ was explained by Walters [48] as spectrum relaxation. The above model are valid for Walters'-B when low memory is considered and $\int_0^\infty \tau^n\lambda(\tau)d\tau, \quad n \geq 2$ are forgone. Based on Eq. (10)-(15), we have the stress components becomes:

$$\tau = \begin{bmatrix}\tau_{xx} & \tau_{xy} \\ \tau_{yx} & \tau_{yy}\end{bmatrix} \tag{16}$$

$$\tau_{xx} = 2\mu_0 \frac{\partial u}{\partial x} - 2k_0\left[u\frac{\partial^2 u}{\partial x^2} + v\frac{\partial^2 u}{\partial x \partial y} - 2\left(\frac{\partial u}{\partial x}\right)^2 + \frac{1}{2}\frac{\partial u}{\partial y}\left(\frac{\partial u}{\partial y} + \frac{\partial v}{\partial x}\right)\right] \tag{17}$$

$$\tau_{yx} = \tau_{xy} = \mu_0\left(\frac{\partial u}{\partial y} + \frac{\partial v}{\partial x}\right) - 2k_0\left[\frac{1}{2}u\left(\frac{\partial^2 u}{\partial x \partial y} + \frac{\partial^2 v}{\partial x^2}\right) + \frac{1}{2}v\left(\frac{\partial^2 u}{\partial y^2} + \frac{\partial^2 v}{\partial x \partial y} - \frac{\partial u}{\partial x}\frac{\partial v}{\partial x} + \frac{\partial u}{\partial y}\frac{\partial v}{\partial y}\right)\right] \tag{18}$$

The analysis of heat transfer depicted in Figure 2 takes place in nature. It includes the three modes of heat transfer which are convection, conduction and radiation. The convection is the transfer of heat through air currents, conduction is the heat transfer through the ground which radiation include the heat transfer from the fire light and the fuel oxidation during the process of combustion.

$$\tau_{yy} = 2\mu_0 \frac{\partial v}{\partial y} - 2k_0 \left[\frac{\partial^2 v}{\partial t \partial x} + u \frac{\partial v}{\partial x \partial y} + v \frac{\partial^2 v}{\partial y^2} - 2 \frac{1}{2} \frac{\partial v}{\partial x} \left(\frac{\partial u}{\partial y} + \frac{\partial v}{\partial x} \right) + \left(\frac{\partial v}{\partial y} \right)^2 \right] \tag{19}$$

The stress tensor above is differentiated to obtain

$$\rho \left(\frac{\partial \tau_{xx}}{\partial x} + \frac{\partial \tau_{xy}}{\partial y} \right) = \mu_0 \left(\frac{\partial^2 u}{\partial y^2} \right) - k_0 \left(v \frac{\partial^3 u}{\partial y^2} + u \frac{\partial^3 u}{\partial x \partial y^2} - 2 \frac{\partial u}{\partial y} \frac{\partial^2 u}{\partial x \partial y} - 3 \frac{\partial u}{\partial x} \frac{\partial^2 u}{\partial y^2} \right) \tag{20}$$

To evaluate the heat flux, the use of Rosseland estimation as explored in Alao *et al.,* [49], Idowu and Falodun [50], Fagbade *et al.,* [51] is required. Hence, q_r in Eq. (2) gives

$$q_r = -\frac{4\sigma_s}{3ke} \frac{\partial T^4}{\partial y} \tag{21}$$

In Eq. (21) above, σ_s signifies Stefan-Boltzmann constant while ke signifies mean absorption coefficient. The difference in temperature existing in the flow are so small that T^4 is expressed as a linear term by employing Taylor series to expand T^4 about T_∞ and forgone higher terms to obtain

$$T^4 \approxeq 4T_\infty^3 T_3 T_\infty^4 \tag{22}$$

Using Eq.(22) in Eq. (21) and employing the outcomes in (3) to obtain:

$$-\frac{\partial q_r}{\partial y} = \frac{16\sigma_s T_\infty^3}{3ke} \frac{\partial^2 T}{\partial y^2} \tag{23}$$

Considering the simplifications of Casson together with Walters-B liquid and substituting Eq. (9), Eq. (20) and Eq. (23) into the governing Eq. (1)-Eq. (3) subject to Eq. (4) and Eq. (5) leads to (see [50] and [51]):

$$\frac{\partial u}{\partial x} + \frac{\partial v}{\partial y} = 0 \tag{24}$$

$$u \frac{\partial u}{\partial x} + v \frac{\partial u}{\partial y} = \frac{\mu_b(T)}{\rho} \left(1 + \frac{1}{\beta} \right) \frac{\partial^2 u}{\partial y^2} + \frac{1}{\rho} \left(1 + \frac{1}{\beta} \right) \frac{\partial u}{\partial y} \frac{\partial \mu_b(T)}{\partial T} \frac{\partial T}{\partial y} + g\beta_t (T - T_\infty) - \frac{\sigma B_0^2}{\rho} u - \frac{k_0}{\rho} \left(v \frac{\partial^3 u}{\partial y^2} + u \frac{\partial^3 u}{\partial x \partial y^2} - 2 \frac{\partial u}{\partial y} \frac{\partial^2 u}{\partial x \partial y} - 3 \frac{\partial u}{\partial x} \frac{\partial^2 u}{\partial y^2} \right) - \frac{\mu_b}{k\rho} \left(1 + \frac{1}{\beta} \right) u \tag{25}$$

$$u \frac{\partial T}{\partial x} + v \frac{\partial T}{\partial y} = \frac{k(T)}{\rho c_p} \frac{\partial^2 T}{\partial y^2} + \frac{1}{\rho c_p} \frac{\partial T}{\partial y} \frac{\partial k(T)}{\partial y} + \frac{16\sigma_s T_\infty^3}{3ke} \frac{\partial^2 T}{\partial y^2} + \frac{\mu_b(T)}{\rho c_p} \left(1 + \frac{1}{\beta} \right) \left(\frac{\partial u}{\partial y} \right)^2 + \frac{Q_0}{\rho c_p} (T - T_\infty) \tag{26}$$

together with the boundary constraints (see Idowu and Falodun [50] and Fagbade *et al.,* [51])

$$u = Bx \quad , v = -v(x) \quad , T = T_w \quad at \quad y = 0 \tag{27}$$

$$u \longrightarrow 0 \quad , T \longrightarrow T_\infty \quad y \longrightarrow \infty \tag{28}$$

u and v represents the relations $u = \frac{\partial \psi}{\partial y}$ and $v = -\frac{\partial \psi}{\partial x}$. The relation $\psi(x, y)$ signifies stream function which satisfies the equation of continuity. The following relations are used for similarity transformation:

$$\eta = \left(\frac{B}{\nu}\right)^{\frac{1}{2}} y \quad , \psi = (\nu B)^{\frac{1}{2}} x f(\eta) \tag{29}$$

We employ the temperature-dependent viscosity alongwith the thermal conductivity presented in Idowu and Falodun [50] as:

$$\mu_b(T) = \mu_b^*[a + b(T_w - T)], \quad k(T) = k^*[1 + \xi(T - T_\infty)] \tag{30}$$

A case where $a = 1$ is used in this paper. Considering equations (26) and (27) and the functions of u and v, Eq. (21)-(23) together with the constraints Eq. (24) andEq. (25) one obtain:

$$\alpha[ff'''' + 2f'f''' + 2f''^2] + \gamma\left(1 + \frac{1}{\beta}\right)[\theta' f'' - \theta f''' + Psf'] + [1 + \gamma]\left(1 + \frac{1}{\beta}\right)[f''' - Psf'] - f'[f' + M_p] + ff'' + G_r\theta = 0 \tag{31}$$

$$((1 + \xi\theta) + \frac{4}{3}R)\theta'' - Prf\theta' + \xi(\theta')^2 + PrEc[1 + \gamma\theta]\left(1 + \frac{1}{\beta}\right)(f'')^2 + Pr\Delta_x\theta = 0 \tag{32}$$

along with the boundary constraints:

$$f' = 1 \quad , f = -S_w \quad , \theta = 1 \quad at \quad \eta = 0 \tag{33}$$

$$f' \longrightarrow 0 \quad , \theta \longrightarrow 0 \quad as \quad \eta \longrightarrow \infty \tag{34}$$

Note that $\gamma = b(T_w - T_\infty), \Delta_x = \frac{Q_0}{B\rho c_p}, Ec = \frac{(Bx)^2}{c_p(T_w - T_\infty)}, Pr = \frac{\nu\rho c_p}{k^*}, R = \frac{4\sigma_s T_\infty^3}{3kek^*}, \xi = \epsilon(T_w - T_\infty), M = \frac{\sigma B_0^2}{\rho B}, Gr = \frac{g\beta_t(T_w - T_\infty)}{B^2 x}, \alpha = \frac{k_0 B}{\nu\rho}, P_s = \frac{\mu^*}{\rho B k}, \beta = \frac{\mu_b\sqrt{2\pi}}{P_y}$ are variable viscosity term, heat generation term, Eckert number, Prandtl number, thermal radiation, varied thermal conductivity, Magnetic, thermal Grashof, viscoelastic parameter, permeability and Casson respectively. The engineering curiosity are the skin friction coefficient (C_f) and local Nusselt number (Nu_x) which are defined by

$$C_f = \frac{\tau_w}{\rho(u_w)^2}, \; Nu_x = \frac{Bxq_w}{K(T_w - T_\infty)}$$

where

$$\tau_w = \left[\mu\left(1 + \frac{1}{\beta}\right)\left(\frac{\partial u}{\partial y}|_{y=0}\right) - \left(2\frac{\partial u}{\partial x}\frac{\partial^2 u}{\partial x \partial y} + 3\frac{\partial u}{\partial x}\frac{\partial^2 u}{\partial y^2}\right)|_{y=0}\right]$$
$$q_w = -K\left(\frac{\partial T}{\partial y}|_{y=0} - \frac{4\sigma_s}{3ke}\left(\frac{\partial T^4}{\partial y}\right)|_{y=0}\right)$$

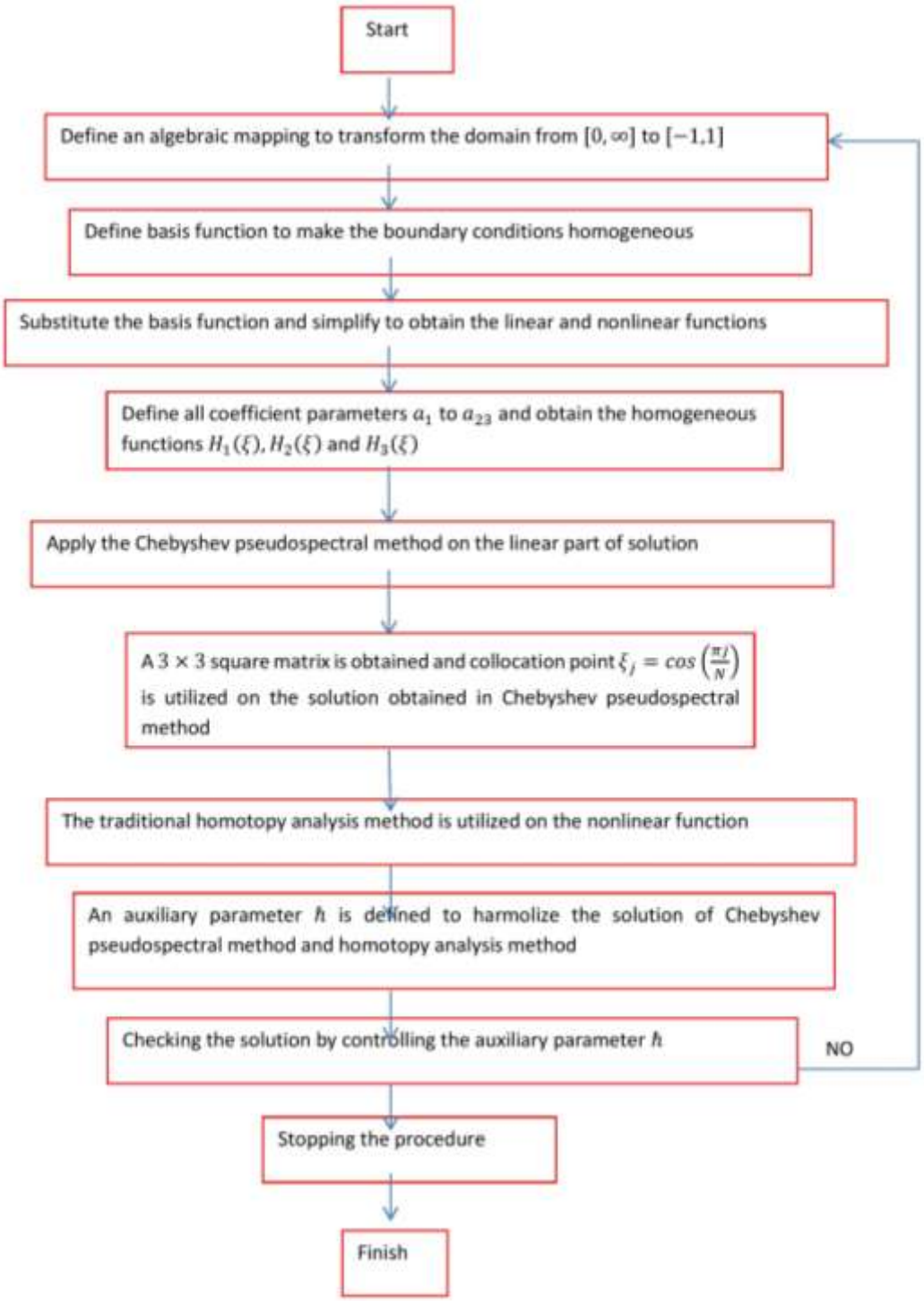

Fig. 2. Flow chart of the numerical approach

3. Method of Solution

3.1 Numerical Analysis

The fourth order coupled nonlinear total differential Eq. (35)-(37) subject to constraints Eq. (38) and Eq. (39) has been solved using SHAM. SHAM is a numerical techniques proposed by Motsa [52]. It combines the techniques of CPM and HAM presented by Liao [53]. To use SHAM, the problem domain is first simplified from $[0, \infty)$ to $[-1,1]$ using the computational domain $[0, L]$. It worth noting

that L signifies length taking to be very large more that thickness of the layers. Due to the transformation of domain, the following algebraic mapping is used on the systems of Eq. (35)-(37) subject to the constraints Eq. (28) and (39).

$$\xi = \frac{2\eta}{L} - 1\,, \quad \xi \in [-1, +1] \tag{35}$$

To use SHAM, the conditions within the boundary are evaluated to be homogeneous using:

$$f(\eta) = f(\xi) + f_0(\eta) \quad , f_0(\eta) = S_w + 1 - e^{-\eta},\ \theta(\eta) = \theta(\xi) + \theta_0(\eta) \quad , \theta_0(\eta) = e^{-\eta} \tag{36}$$

and $f_0(\eta)$ and $\theta_0(\eta)$ are guesses at the initial chosen in conformity with the constraints at the boundary $f(\eta)$ and $\theta(\eta)$ respectively. Using Eq. (33) on the simplified Eq. (28) and (29) along the boundary constraints Eq. (30) and Eq. (31) leads to:

$$\gamma\left(1+\frac{1}{\beta}\right)[\theta' f'' - \theta f''' + Psf'] + [1+\gamma]\left(1+\frac{1}{\beta}\right)[f''' - Psf'] + f''[a_2 + f + a_4 + a_{12} + 2\alpha f''] + \theta[a_6 + Gr] + f'[a_{10} - M_p + a_5] + f[a_3 + a_8] + f''''[\alpha f + a_9] + f'''[2\alpha f' + a_7 + a_{11}] + a_1\theta' - (f')^2 = \psi_1(\eta) \tag{37}$$

$$\left(\left(1+\frac{4}{3}R\right) + \xi\theta + b_2\right)\theta'' - (Prf + b_4 + \theta' + b_5)\theta' + (b_1 + b_8 + Pr\Delta_x)\theta + b_3 f + \left(PrEc(1+\gamma)\left(1+\frac{1}{\beta}\right) - PrEc\gamma\theta\left(1+\frac{1}{\beta}\right) + b_9\right)(f'')^2 + (b_6 + b_7\theta + b_1)f'' = \psi_2(\eta) \tag{38}$$

subject to

$$f(-1) = f(1) = f'(-1) = f'(1) = 0 \quad , \theta(-1) = \theta(1) = 0 \tag{39}$$

where

$$a_1 = \gamma\left(1+\frac{1}{\beta}\right)f_{0,,} \quad , a_2 = \gamma\left(1+\frac{1}{\beta}\right)\theta'_0 \quad , a_3 = f''_0 \quad , a_4 = f_0 \quad , a_5 = -2f'_0,$$
$$a_6 = -\gamma\left(1+\frac{1}{\beta}\right)f'''_0,\ a_7 = -\gamma\left(1+\frac{1}{\beta}\right)\theta_0,\ a_8 = \alpha f''''_0,\ a_9 = \alpha f_0 \text{ M}$$
$$a_{10} = 2\alpha f'''_0, \qquad a_{11} = 2\alpha f'_0, \qquad a_{12} = 4\alpha f''_0$$
$$\psi_1(\eta) = f'_0\left[M_p + [1+\gamma]\left(1+\frac{1}{\beta}\right)Ps - \gamma\left(1+\frac{1}{\beta}\right)Ps\right] - f'''_0\left[(1+\gamma)\left(1+\frac{1}{\beta}\right) - \gamma\left(1+\frac{1}{\beta}\right)\theta_0 + 2\alpha f'_0\right] - f''_0\left[\gamma\left(1+\frac{1}{\beta}\right)\theta'_0 + f_0\right] + (f')^2 - Gr\theta_0 - \alpha f_0 f''''_0$$
$$b_1 = \xi\theta''_0, \qquad b_2 = \xi\theta_0, \qquad b_3 = -Pr\theta'_0, \qquad b_4 = -Prf_0, \qquad b_5 = 2\theta'_0,$$
$$b_6 = 2PrEc[1+\gamma]\left(1+\frac{1}{\beta}\right)f''_0, b_7 = -2PrEc\left(1+\frac{1}{\beta}\right)\gamma f''_0,$$
$$b_8 = -PrEc\gamma\left(1+\frac{1}{\beta}\right)(f''_0)^2, b_9 = -PrEc\gamma\left(1+\frac{1}{\beta}\right)\theta_0, b_{10} = -2PrEc\gamma\left(1+\frac{1}{\beta}\right)\theta_0 f''_0$$
$$\psi_2(\eta) = -\left(1+\frac{4}{3}\right)\theta''_0 - \xi\theta_0\theta''_0 + Prf_0\theta'_0 - \xi\theta'_0\theta'_0 - PrEc[1+\gamma]\left(1+\frac{1}{\beta}\right)(f''_0)^2 + PrEc\left(1+\frac{1}{\beta}\right)\gamma\theta_0(f''_0)^2 - Pr\Delta_x\theta_0$$

To solve the resulting Eqs. (37) and (38), CPM is applied and $f(\xi), \theta(\xi)$ and $\phi(\xi)$ are evaluated as a shortened series of Chebyshev polynomials:

$$f(\xi) \approx \sum_{k=0}^{N} f_k T_k(\xi_j) \quad , \theta(\xi) \approx \sum_{k=0}^{N} \theta_k T_k(\xi_j) \quad , j = 0,1,2,\ldots,N \tag{40}$$

and $\xi_0, \xi_1, \chi_2, \ldots, \xi_N$ are points of collocation in Gauss-Lobatto (Canuto *et al.,* [54]) denoted by $\xi_j = cos\frac{\pi j}{N} \quad , j = 0,1,2,\ldots,N$, T_k is the k^{th} Chebyshev polynomial where $N+1$ signifies collocation points number. The functions $f(\eta), \theta(\eta)$ and $\phi(\eta)$ derivatives at the points of collocation are given as

$$\frac{d^r f}{d\eta^r} = \sum_{k=0}^{N} D_{kj}^r f(\xi) \quad , \frac{d^r \theta}{d\eta^r} = \sum_{k=0}^{N} D_{kj}^r \theta(\xi)$$

where r signifies differential order and $D = \frac{2}{L} D$ (see Canuto *et al.,* [54]) with D signifies Chebyshev differential matrix. The parameter $\bar{h}$ is chosen to know the SHAM convergency. It controls the SHAM convergence series outcomes. During computations, an incremental value of $\bar{h}$ result to autonomous results. Thus, the value of $\bar{h}$ utilized as $\bar{h} = 0.2$ at $L = 12$ and the collocation point number is $N = 120$.

To solve the resulting Eq. (34) and Eq. (35), CPM is applied and $f(\xi), \theta(\xi)$ and $\phi(\xi)$ are evaluated as a shortened series of Chebyshev polynomials:

$$f(\xi) \approx \sum_{k=0}^{N} f_k T_k(\xi_j) \quad , \theta(\xi) \approx \sum_{k=0}^{N} \theta_k T_k(\xi_j) \quad , j = 0,1,2,\ldots,N$$

and $\xi_0, \xi_1, \chi_2, \ldots, \xi_N$ are points of collocation in Gauss-Lobatto (Canuto *et al.,* [54]) denoted by $\xi_j = cos\frac{\pi j}{N} \quad , j = 0,1,2,\ldots,N$, T_k is the k^{th} Chebyshev polynomial where $N+1$ signifies collocation points number. The functions $f(\eta), \theta(\eta)$ and $\phi(\eta)$ derivatives at the points of collocation are given as

$$\frac{d^r f}{d\eta^r} = \sum_{k=0}^{N} D_{kj}^r f(\xi) \quad , \frac{d^r \theta}{d\eta^r} = \sum_{k=0}^{N} D_{kj}^r \theta(\xi) \tag{41}$$

where r signifies differential order and $D = \frac{2}{L} D$ (see Canuto *et al.,* [51]) with D signifies Chebyshev differential matrix. The parameter $\bar{h}$ is chosen to know the SHAM convergency. It controls the SHAM convergence series outcomes. During computations, an incremental value of $\bar{h}$ result to autonomous results. Thus, the value of $\bar{h}$ utilized as $\bar{h} = 0.2$ at $L = 12$ and the collocation point number is $N = 120$.

3.2 Statistical Analysis

The procedures of linear and quadratic regressions employed in this study are as follows (see Memon *et al.,* [55]).

$$\text{Mean: } \bar{x} = \frac{\sum x_i}{n}, \quad \bar{y} = \frac{\sum y_i}{n} \text{ and } \bar{x}^2 = \frac{\sum x_i^2}{n} \Big\} \tag{42}$$

Hence,

$$S_{xx} = \sum x_i^2 - n\,\bar{x}^2, \quad S_{xy} = \sum x_i y_i - n\bar{x}\bar{y}, \quad S_{xx^2} = \sum x_i^2 - n\bar{x}\bar{x}^2\,, \quad S_{x^2x^2} = \sum x_i^4 - n\bar{x}^2\bar{x}^2 \tag{43}$$

The study precedes the analysis of best quadratic fit using the equation:

$$Y = C + Bx + Ax^2 \tag{44}$$

Here A, B, and C are calculated by employing:

$$B = \frac{S_{xx}S_{x^2x^2} - S_{x^2y}S_{xx^2}}{S_{xx}S_{x^2x^2} - \left(S_{xx^2}\right)^2}, \quad A = \frac{S_{x^2y}S_{xx} - S_{xy}S_{x^2x}}{S_{xx}S_{x^2x^2} - \left(S_{xx^2}\right)^2} \quad and \quad C = \bar{y} - B\bar{x} - C\bar{x}^2 \tag{45}$$

To analyse the linear regression to fit the straight line equation is defined as:

$$y = a + bx \tag{46}$$

where a and b are defined as follows:

$$a = \frac{\sum(x_i - \bar{x})(y_i - \bar{y})}{\sum(x_i - \bar{x})^2}, \quad b = \bar{y} - a\bar{x} \tag{47}$$

The linear and quadratic regressions are further explained in this study to estimate the reduced Nusselt number to examine the impact ofNb and Nt (see Ayub *et al.,* [56] and Jahan *et al.,* [57]). The corrections linear and quadratic regressions are defined as follows:

$$Nu_{est} = Nu_r + C_b Nb + C_t Nt \tag{48}$$
$$Nu_{est} = Nu_r + C_b Nb + C_t Nt + C_{bb} Nb^2 + C_{tt} Nt^2 + C_{bt} NbNt$$

where coefficients of linear and quadratic regressions are C_b, C_t, C_{bb}, C_{tt} and C_{bt} respectively. The regression equations are valid within the range [0, 0.5]. The expected maximum error is gotten using

$$\epsilon_2 = \frac{|Nu_{est} - Nu|}{|Nu|} \tag{49}$$

4. Results and Discussion

A novel, accurate and elegant numerical spectral base method called SHAM has been utilized on the fourth-order total differential Eqs. (31) and (32) subject to (33) and (34). To explain the physical problem shown in Figure 1, the behaviour of controlling parameters is plotted for velocity as well as the temperature of the boundary layer. Effects of flow parameters on engineering curiosity such as local skin friction coefficient plus Nusselt number are calculated and presented in a table. Therefore, all computations in the present study correspond to these default values unless it is otherwise stated.

4.1 Validation of Results from Numerical Experiment

To ascertain the correctness of the programming code used in this study, parameters such as γ, Ps, ξ, β, α, and Δ_x are set to zero to validate with the study of Fagbade *et al.,* [48] while α, β, and Δ_x

are set to zero to validate with the published work of Salawu and Dada [43]. The comparison as shown in Table 1 and Table 2 are in good agreement.

Table 1
Numerical calculations of skin friction coefficient (C_f) and Nusselt number (Nu) for different values of α and M

		Fagbade *et al.,* [48]				Present study			
		$S_w = -0.5, R = 0$		$S_w = 0, R = 0.5$		$S_w = -0.5, R = 0$		$S_w = 0, R = 0.5$	
α	M	C_f	Nu	C_f	Nh	C_f	Nu	C_f	Nu
0.0	0.0	1.02012	1.12032	0.45788	1.15242	1.02010	1.12030	0.45786	1.15240
	0.5	1.59439	1.03511	1.12882	1.01474	1.59437	1.03510	1.12880	1.01472
	1.0	2.08219	0.97811	1.67946	0.92332	2.08219	0.97810	1.67944	0.92330
0.01	0.0	1.02979	1.12070	0.39329	1.15842	1.02977	1.12068	0.39327	1.15840
	0.5	1.71062	1.02916	1.16601	1.01388	1.71060	1.02814	1.16600	1.01386
	1.0	2.29355	0.96779	1.80546	0.91748	2.29353	0.96777	1.80544	0.91746

Table 2
Numerical calculations of Nusselt number (Nu) for distinct values of Pr as compared to Salawu and Dada [43]

Pr	Salawu and Dada [43]	Present study
0.7	-0.456049	-0.456047
1.0	-0.582225	-0.582225
10.0	-2.307950	-2.307951
5.0	-4.028228	-4.028227

4.2 Discussion on Tables of Numerical Value

The variation of the viscoelastic parameter (α), Casson parameter (β), permeability parameter (Ps), variable viscosity parameter (γ), magnetic parameter (Mp), Grashof parameter (Gr), variable thermal conductivity parameter (ξ), thermal radiation parameter (R), Prandtl number (Pr), Eckert number (Ec), heat generation parameter (Δ_x) on skin friction and Nusselt number is contained in Table 3.

The numerical experiment showed that an increase improves the hydrodynamic and thermal boundary layer by increasing skin friction and the Nusselt number. This implies that the Walters-B fluid is moving quickly, and as a result, the rate of heat transfer increases. It was observed that an increase in the Casson parameter is observed to decrease local skin friction due to the presence of plastic dynamic viscosity in Casson fluid and the imposed magnetic parameter. On the order hand, it is observed to increase the rate of heat transfer by increasing the Nusselt number. In Table 3, an increase in Ps allows fluid particles to flow by increasing skin friction and the entire hydrodynamic boundary layer. The rate of heat transfer increases as a result of fluid-particle collisions. The thermo-physical properties are assumed to vary within the boundary layer in this analysis. The computational results showed that a higher value accelerates the momentum gathered by fluid particles and the rate of heat transfer. This is because as the variable viscosity parameter increases, so does the local skin friction and Nusselt number. More so, increasing the magnetic parameter (Mp) reduces local skin friction while increasing the rate of heat transfer. This causes an electromagnetic force to be generated, which slows fluid motion within the hydrodynamic and thermal boundary layers.

Further investigation revealed that increasing the thermal Grashof number improves the local skin friction and Nusselt number. An external force acts on the fluid physically such as electromagnetic and gravitational forces help to improve the behavior of fluids within the

hydrodynamic and thermal boundary layers. The influenceincreasing the variable thermal conductivity parameter improves local skin friction and the Nusselt number. The fluid particles warm up as the thermal conductivity changes, increasing the rate of thermal dissipation. Thermal radiation is observed in Table 3 to raise the temperature of fluids within the boundary layer. Thermal radiation improves convective flow and is employed in the design of many energy conversion systems that operate at higher temperatures. Our predictions showed that increasing Pr reduces local skin friction while increasing the Nusselt number. This demonstrates an extremely high kinematic viscosity. A fluid with a higher Pr has a higher viscosity, which reduces local skin friction as Pr increases. Likewise, increasing Ec accelerates the local skin friction and Nusselt number. The Eckert number explains how kinematic energy is converted to internal energy. As a result, greater viscous dissipation results in a larger hydrodynamic and thermal boundary layer. Upheaving heat generated in the proximity of boundarylayer improves the hydrodynamic and thermal boundary layer. This is due to an increase in local skin friction and Nusselt number as the heat generation parameter is increase.

This result finds application in the processing of food because when the environment or a container where food raw materials are stored has too much heat or has its environment to be hot, it tends to decrease the food content. For example, consider that concentrated fruit juice is subjected to heat, it reduces its content and the juice will ferment at a high temperature to give a sour taste. This means that the presence of heat has reduced its content. Physically, explains the fact that the viscosity of the fluid is related directly to itself but inversely to the yield stress. Thus, decreases the momentum layer thickness together with the fluid velocity the moment Casson parameter increases.

Table 3
Contributions of α , β, Ps, γ , M_p, Gr, ξ , R, Pr, Ec, and Δ_x on the local skin friction (C_f) and Nusselt number

α	β	Ps	γ	M_p	Gr	ξ	R	Pr	Ec	Δ_x	C_f	Nu
0.3											2.94771957	0.97024345
0.6											3.15283398	0.97153534
0.9											3.38058653	0.97269802
	1.0										4.11114174	0.96697420
	2.0										3.79976804	0.96857450
	3.0										3.53062120	0.96998729
		0.2									1.91185811	0.97999413
		0.4									1.92870466	0.98026662
		0.6									1.94852704	0.98051926
			2.0								1.64209878	0.97590167
			3.0								1.80551289	0.97679253
			4.0								1.98028248	0.97759578
				0.5							1.19087682	0.71712993
				1.0							1.07980241	0.74407269
				2.0							0.97654786	0.76897016
					0.0						1.06949269	0.76430078
					0.5						1.17932625	0.78592437
					1.0						1.29741996	0.80591614
						2.0					1.38842518	0.88674581
						3.0					1.52626413	0.89600813
						4.0					1.67404495	0.90458920
							1.0				1.20080771	0.81847858
							2.0				1.32144838	0.83442731
							3.0				1.45102077	0.84918782
								0.71			2.33842056	0.76430078
								1.0			2.14571376	1.97694861
								3.0			1.96544037	1.97762833

0.01		1.64832600	0.79690227
0.02		1.81233839	0.80616845
0.03		1.98778880	0.81431762
	0.5	1.65166351	0.63551012
	1.0	1.81600436	0.65187552
	2.0	1.99181270	0.66655010

Figure 3b depicts the in influence of Walters-B liquid (α) on the velocity plot. It is observed that an increment in (α) corresponds to an enhancement in the velocity plot. In the domain $0 \leq \eta \leq 12$, an increase in α means an increment in the velocity closely to the plate. Hence, at the ambient vicinity where the temperature is high, the effect of increasing α is negligible. The buoyancy force accelerates the velocity and dominates the entire boundary layer surface and brings an increment to the fluid velocity right starting from the porous plate to the ambient vicinity at $\eta \longrightarrow \infty$. An increased $\xi = \gamma(T_w - T_\infty)$ means a hike in the momentum layer thickness within the fluid domain. Figure 3c represents the in influence of the Darcy law of porosity considered in this study. Increasing the porosity term (Ps) is detected to increase the fluid velocity graph. It should be noted that the porosity of the flow geometry is expected to affect the velocity of the two fluids at the wall the moment they mixed together. Their mixture increases the velocity of the fluid as shown in figure 3c because increasing the hole makes the Casson and Walters-B liquid to mix together more and thereby enhances the fluid motion.

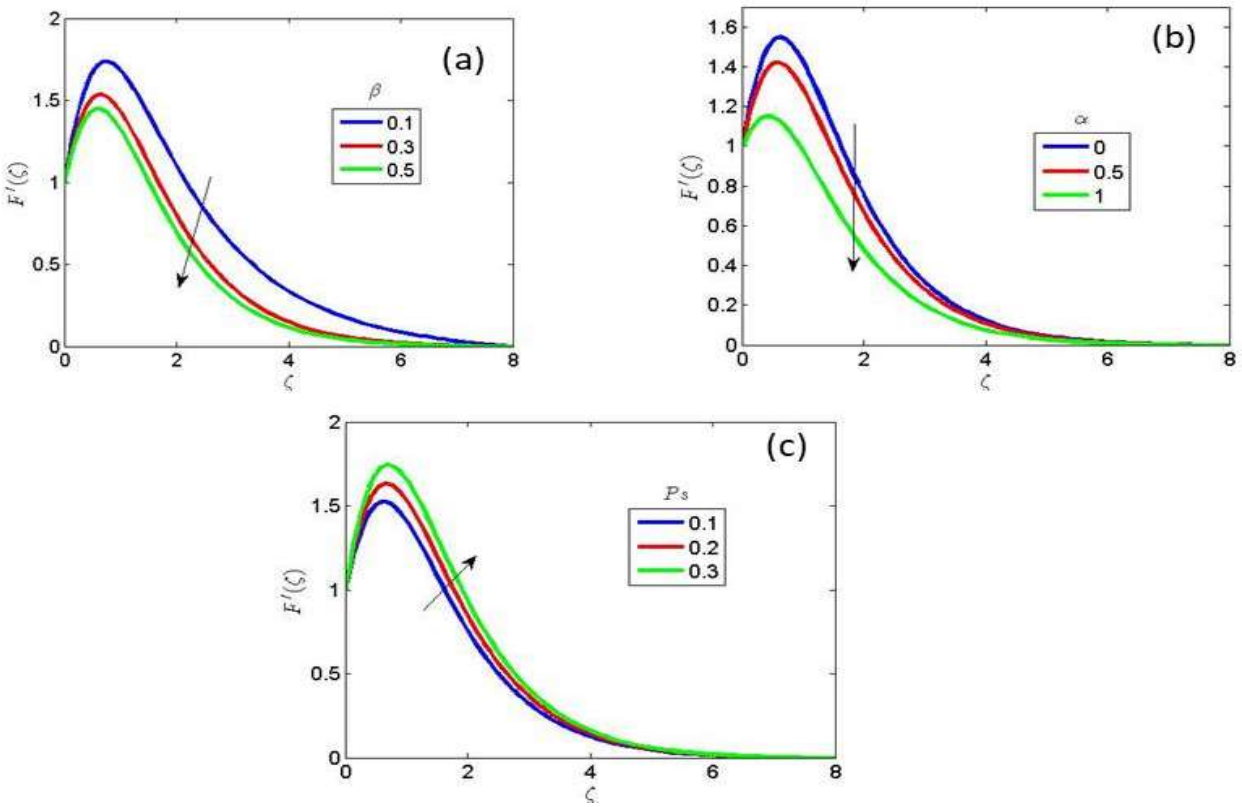

Fig. 3. Velocity distribution under β, α and Ps

Figure 4a portrays the influence of thermal Grashof number on the velocity plot. The presence of dimensionless Grashof number (Gr) in fluid flow gives rise to a force called buoyancy force. It is important to explain that $Gr > 0$ means generative buoyancy force while $Gr < 0$ means destructive buoyancy. Hence, increasing Gr as shown in figure 4a brings an increase to the fluid velocity profile. In a practical sense, pressure increases the same way as its depth. Note that the pressure at the lower

side of the object is more than the force at the upper side. Figure 4b explains how the imposed magnetic field strength affects the fluid velocity profile. The imposed magnetism of strength (B_0) gives rise to Lorentz force. Now, increasing the value of magnetic parameter (M) increases the strength of this force. Note that Lorentz force drags the liquid flow of an electrically conducting fluid and degenerate its motion. The presence of Lorentz force as well as varying the fluid viscosity and its thermal conductivity,the fluid velocity throughout the flow domain. When $M = 0$, it means the absence of transverse velocity and thereby induces hall currently.

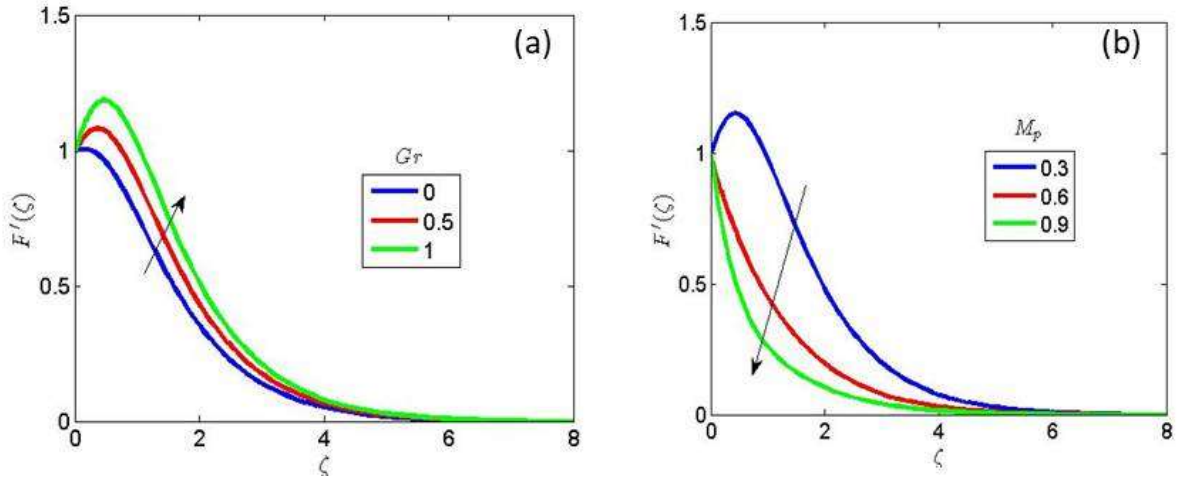

Fig. 4. velocity distribution under Grashoff effect and magnetic field

Figure 5a and Figure 5b portrays the thermal radiation (Ra) effect on the velocity and temperature plots respectively. Radiation is an approach of heat transport which does not require a particles to transport the heat energy. This means that radiation as a means of heat transport does not need any material to transport thermal conductivity. Figure 2 shows the transport of heat from a burning Sherwood to the hand of human being. In figure 2, it is obvious that the heat from the Sherwood is transferred directly to the hand without any material medium. A higher radiation parameter is seen to raise the velocity together with the temperature profile. The thermal radiation parameter plays an important role in a territory where temperature is high. It helps to boast the thermal situation of the fluid domain. This means that wherever Ra is increased in heat and mass transport processes, it added heat energy to the thermal layer. In a practical sense, adding heat energy to flow elevate the temperature of the liquid. Our experiment shows that more value of Ra enhances the velocity plot, temperature plot, hydrodynamic and thermal layer thickness. From Figure 1, the free stream environment is considered to be hot temperature and also thermally-stratified medium. Hence, increasing Ra add more temperature to this free stream environment. This means that, the non-Newtonian fluids posses a very high temperature from the wall to the free stream.

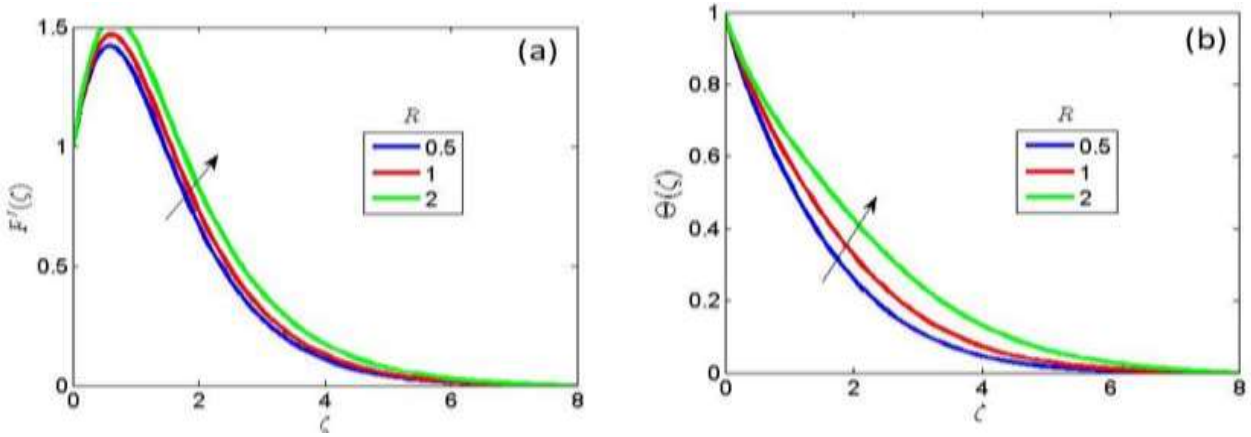

Fig. 5. Outcome of Ra on the (a) velocity (b) temperature graph

Figure 6a and Figure 6b depicts the effect of the heat generation (Δ_x) on the velocity and temperature plots respectiveely. An increase in (Δ_x) causes the velocity and temperature plots to rise. In practice, when atoms and molecules move, they generate thermal energy. Heat is produced in the form of electromagnetic radiation. Physically, increasing (Δ_x) generates heat both at the boundary and in the surrounding environment. In fact, the ambient environment is thermally stratified and hot at the same time, so increasing (Δ_x) produces a spontaneous heat energy that increases the thickness of the thermal layer. Furthermore, increasing the momentum and thermal layer thickness will intensify the temperature and heat condition of the liquid by increasing the product of liquid density and specific heat at constant pressure.

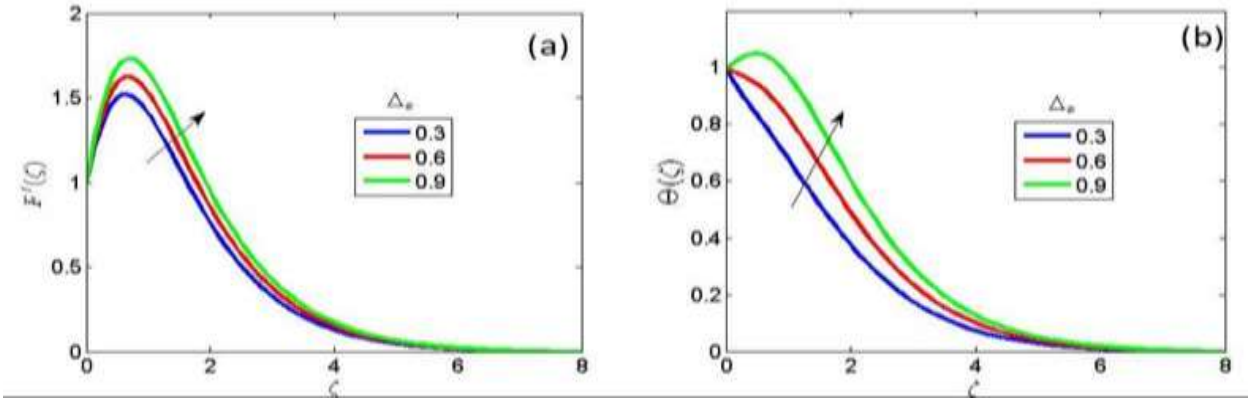

Fig. 6. Outcome of Δ_x on the (a) velocity (b) temperature graph

Figure 7a and Figure 7b depicts the impact of the viscous dissipative parameter (Eckert number (Ec)) on the velocity and temperature profiles respectively. Thiese figures shows that increasing Ec improves both the fluid velocity plot and the temperature plot. The dimensionless number Ec is calculated by adding a term for viscous dissipation to the energy equation. Ec depicts the relationship that exists between kinetic energy and enthalpy in liquid motion. Increase in Ec strengthens fluid shear forces. As shown in Figure 7, increasing the value of Ec by varying the viscosity with thermal conductivity raises the fluid velocity and temperature. Because of frictional heating, Ec generates heat energy in motion, resulting in an increase in momentum alongwith thermal boundary layer thickness. Figure 8a and Figure 8b depicts the contribution of the Prandtl number (Pr) on the velocity and temperature plots. As the value of Pr increases, the velocity and temperature plot becomes degenerate. This is due to the fact that higher Pr produces a lot of viscosity, which causes the liquid velocity profile to degenerate. In this study, where fluid viscosity and thermal conductivity vary and

the free stream environment is hot and thermally stratified, a high Pr value corresponds to a decrease in temperature and thickness of the fluid thermal boundary layer. As a result, the fluid becomes conducive when Pr graduate to a unity value mgnitude.

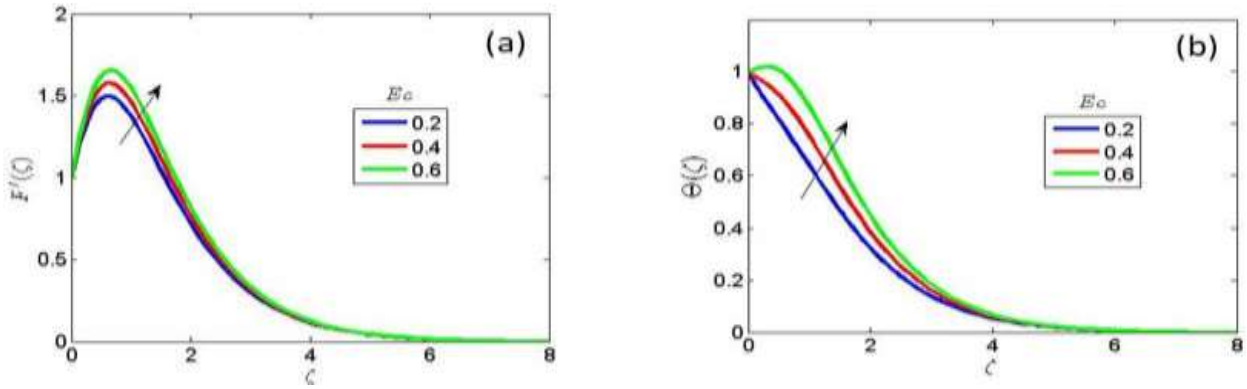

Fig. 7. Outcome of Ec on the (a) velocity (b) temperature graph

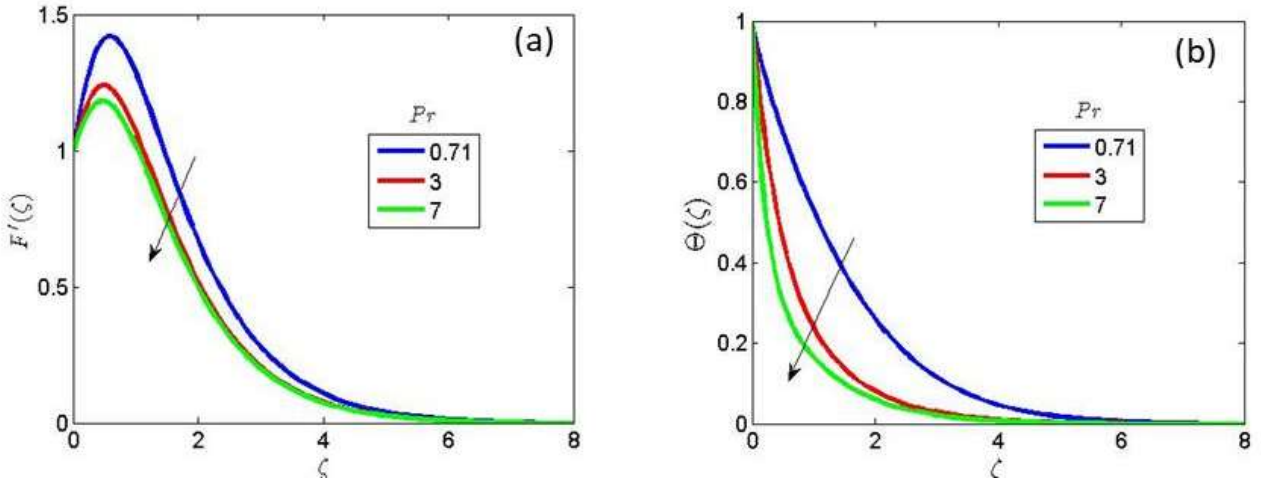

Fig. 8. Outcome of Pr on the (a) velocity (b) temperature graph

The contribution of variable viscosity (γ) on the velocity and temperature profile is depicted in Figure 9a and Figure 9b A high value of is observed to raise the velocity and temperature profiles. Physically, large aids in the movement of fluid particles within the boundary layer. Increase in drastically raises the temperature profile right from the wall to the free stream, where thermal stratification and a hot environment influence the flow (Figure 9). Furthermore, the injected $(\gamma = \epsilon = 6)$ causes an increase in the overall momentum and thermal boundary layer thickness. Figure 10 depicts the outcome of varying variable thermal conductivity values. Because of the injected $(\gamma = \epsilon = 6)$, the effect of variable thermal conductivity parameter (γ) on velocity and temperature is observed to increase momentum and thermal boundary layer thickness. Because of the injected variable viscosity and thermal conductivity (i.e. ==6), the hot environment, and the thermally-stratified medium, the fluid velocity increases close to the wall, as shown in Figures 9 and 10. Furthermore, the velocity profile far away from the plate increases slightly. This is due to the Darcy law of porosity, which is being considered in this study.

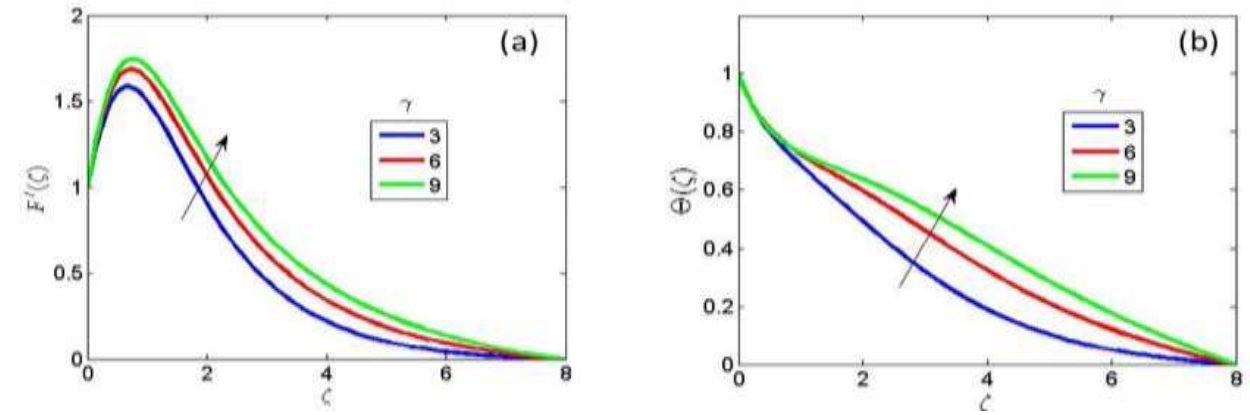

Fig. 9. Outcome of γ on the (a) velocity (b) temperature graph

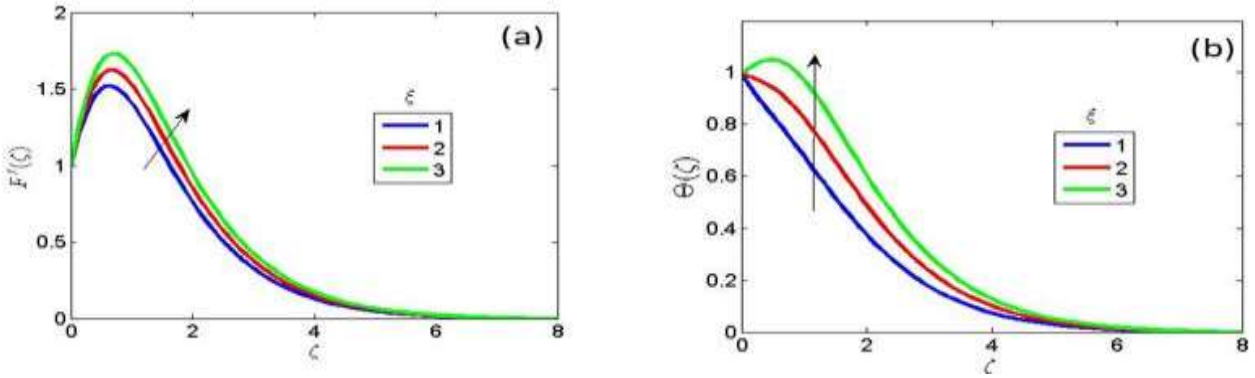

Fig. 10. Outcome of ξ on the (a) velocity and (b) temperature graph

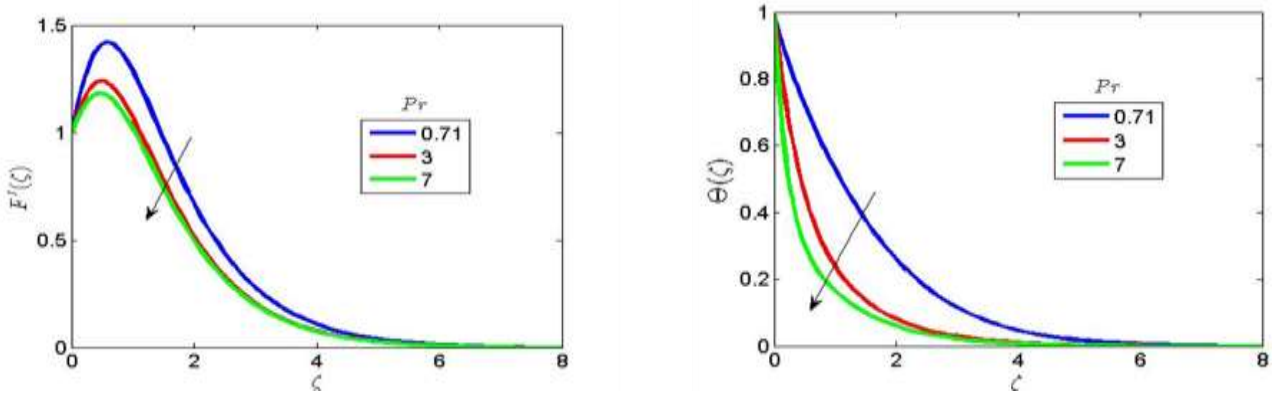

(a) (b)

Fig. 11. Outcome of Pr on the (a) velocity (b) temperature graph

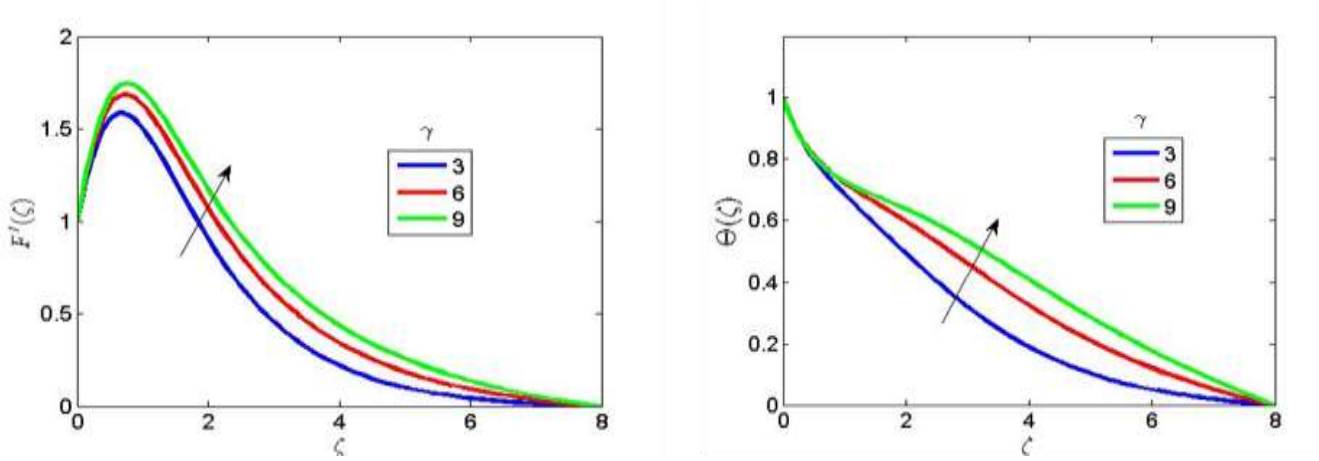

(a) (b)

Fig. 12. Outcome of γ on the (a) velocity (b) temperature graph

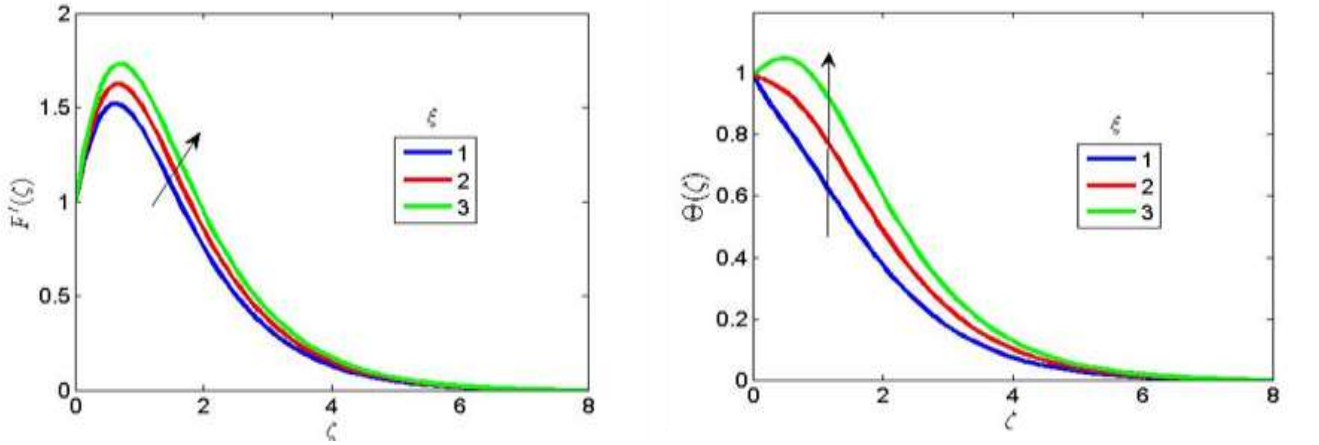

(a) (b)

Fig. 13. Outcome of ξ on the (a) velocity and (b) temperature graph

4.3 Discussion of 2D Statistical Graphs of Parameters on Physical Quantities

Figure 14 illustrates the statistical analysis of α on the skin friction and Nusselt number. From figure 14, a higher value of α enhances the skin friction but has a minimal effect on the Nusselt number. Figure 15 shows that a higher value of β reduces the skin friction while it is negligible on the Nusselt number. This is due to the plastic dynamic viscosity which ascends the flow of fluids (Casson-Walters-B) by lowering the hydrodynamic boundary layer. The reaction of Ec on skin friction and Nusselt number is depicted in Figure 16. In the Figure 16, a higher value of Ec raises the skin friction and minimal reaction on the Nusselt number. A higher viscous dissipative heat results to higher temperature by raising the thermal boundary layer. Higher variable viscosity (γ) as illustrated in Figure 17 is noted to increase the skin friction and Nusselt number. The values of skin friction are 1.01, 1.18, and 1.23 while Nusselt numbers are 0.68, 0.69 and 0.8 for a higher thermal Grashof number as shown in Figure 18. This shows that the buoyancy force parameter shot up the hydrodynamic and thermal boundary layer thickness. A higher magnetic parameter against skin friction as follows: Mp=0.5 gives skin friction of 1.19, Mp=1.0 gives skin friction of 1.08, Mp=2.0 gives skin friction of 0.89. This shows a decreased skin friction for higher values of Mp. A higher Mp is also noted to raise the Nusselt number. In Figure 20, when Pr=0.71 the skin friction is 2.47, when Pr=1.0 the skin friction is 2.21, when Pr=3.0 the skin friction is 1.59 while as Pr=0.71 the Nusselt number is 0.55, when Pr=1.0 the Nusselt number is 1.59 while Pr=3.0 the Nusselt number is 1.599. This shows

a lower skin friction and higher Nusselt number as the values of Pr increases. An increase in the thermal reaction is observed to elevates the skin friction and the Nusselt number in Figure 21. In Figure 22, a higher variable thermal conductivity is observed to drastically increase the skin friction while a minimal reaction is noticed on the Nusselt number. Figure 22 shows the total agreement of the present study with the published work of Salawu and Dada [43].

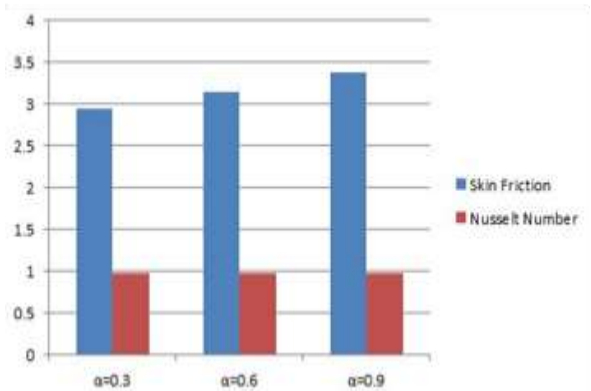

Fig. 14. Statistical analysis of α reaction on the Skin friction and Nusselt number

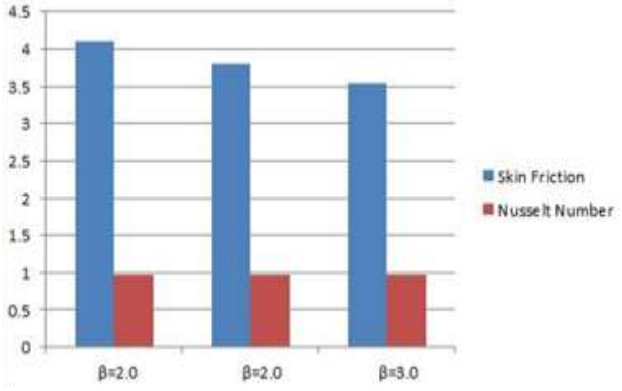

Fig. 15. Statistical analysis of β reaction on the Skin friction and Nusselt number

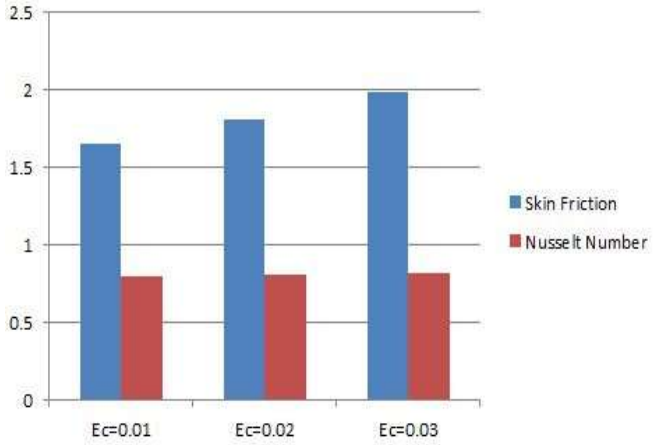

Fig. 16. Statistical analysis of Ec reaction on the Skin friction and Nusselt number

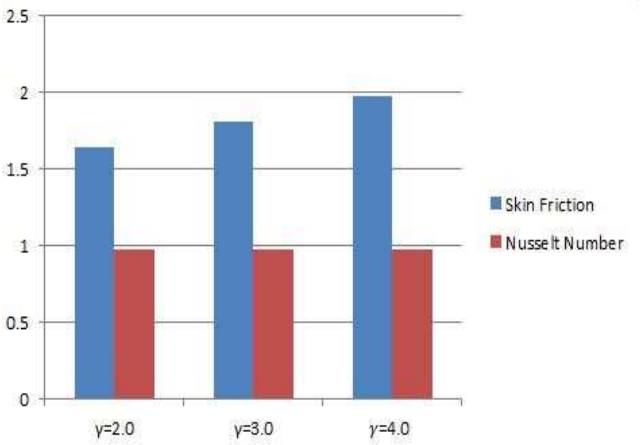

Fig. 17. Statistical analysis of γ reaction on the Skin friction and Nusselt number

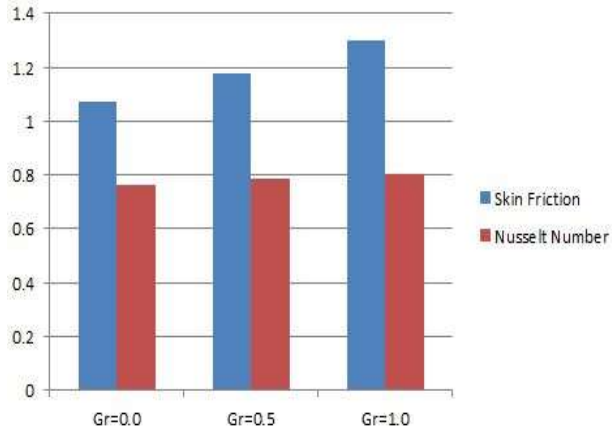

Fig. 18. Statistical analysis of Gr reaction on the Skin friction and Nusselt number

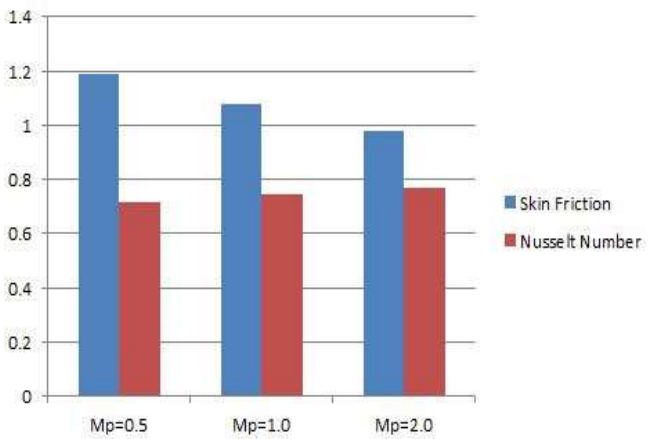

Fig. 19. Statistical analysis of Mp reaction on the Skin friction and Nusselt number

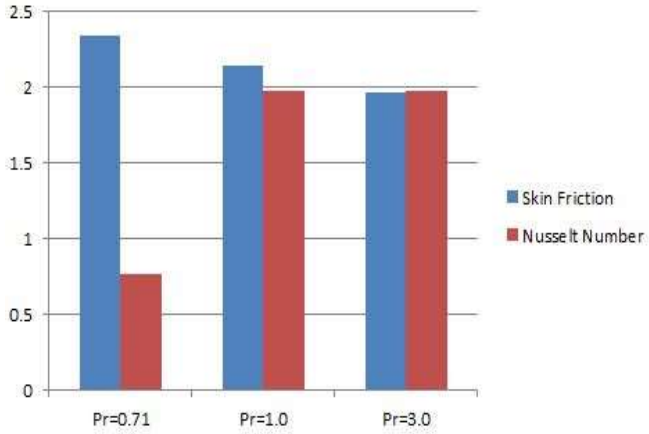

Fig. 20. Statistical analysis of Pr reaction on the Skin friction and Nusselt number

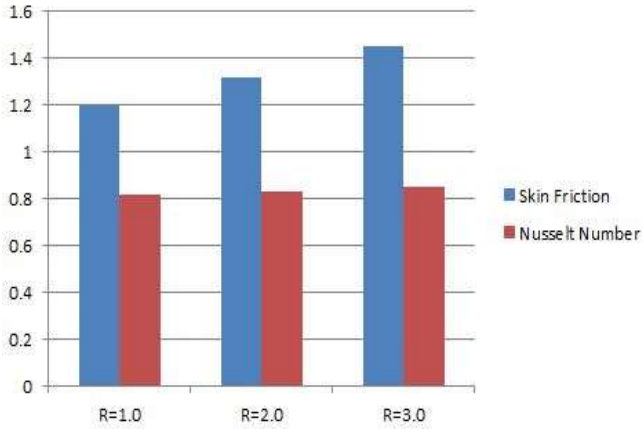

Fig. 21. Statistical analysis of R reaction on the Skin friction and Nusselt number

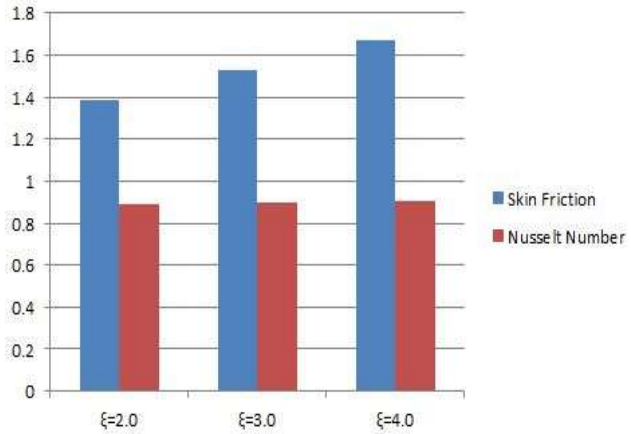

Fig. 22. Statistical analysis of ξ reaction on the Skin friction and Nusselt number

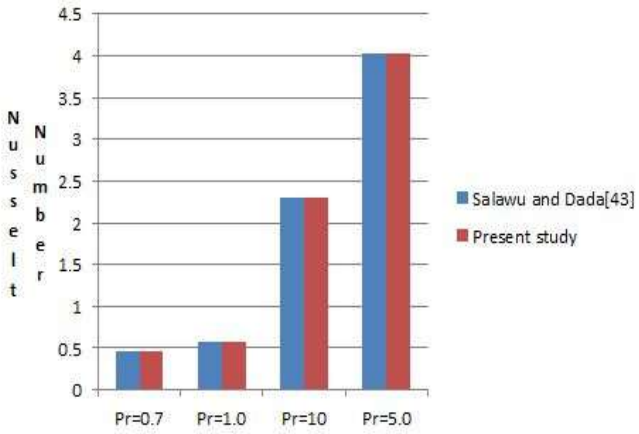

Fig. 23. Statistical analysis of the present and the published work of Salawu and Dada [43]

5. Conclusions

The flow behavior of Casson and Walters-B liquid fluids was investigated together in this study. The Casson, Tomatoe, and Walters-B liquids are ceramic processing, polymethyl methacrylate, and chromatography, respectively. This study clarifies the physical scenario that underlies the simultaneous flow of Casson and Walters-B liquid fluids in a vertical porous plate. These fluids are mixed together in the boundary layer, and as they flow towards a hotter environment, the fraction of Walters-B decreases as the temperature difference increases $(i.e\ T_w - T_\infty)$. The major findings in this study are:

i) The fluid mobility is found to be hampered by the magnetic field strength because the viscosity and heat conductivity are both considered;
ii) In this study, the free stream environment is assumed to be hot, and hence an increase in the thermal radiation parameter promotes degeneration in this environment with limited fluid movement;
iii) As illustrated in figure 1, the applied magnetic field strength (B_0) causes Lorentz force, which slows the flow fluid velocity and reduces the thickness of the boundary layer.
iv) Increases in the permeability parameter allow more Casson and Walters-B liquid fluid flow to enter, resulting in an increase in the intensity of the fluid flow. As a result, there is more

heat at the boundary layer, and the heat at the free stream, where the environment is heated, continues to rise;

v) Increase in the heat generation parameter was observed to increase the velocity and temperature profiles. This also affect the thickness of hydrodynamic and thermal boundary layer.

It is envisaged that the findings of this study will be valuable in food processing, drilling operations, and bioengineering. Oil-pipeline friction reduction and surfactant applications to large-scale heating and cooling systems are the most common practical applications. It may also be used to improve flow in petroleum pipelines by adding high-polymer additives, which is particularly helpful for commercial applications. The effects of Soret and Dufour on fluid flow are profound, and they have applications in engineering, such as isotope separation. The current study has a significant impact on science and technological applications. Industrial polymers like polymethly methacrylate, chromatography fluid, and ceramic processing fluid are examples of Walters-B viscoelastic fluids. Agriculture, communication hardware appliances, and bio-medical applications all use them. Concentrated fruit juice and jelly are also examples of Casson fluid addressed in this study. As a result, polymer production, ceramics or glassware manufacturing, particle deposition onto wafers in the microelectronics industry, polymer engineering, metallurgy, magnetically controlled metal welding or magnetically controlled metal coating of metals, and other fields are all interested in this finding. In comparison to the other approaches in the literature evaluated in this study, the SHAM was shown to be more efficient due to its flexibility in the use of linear operators. As a result, SHAM was chosen due of its elegance and precision.

References

[1] Sun, Xiang, Guang-Wei Zhu, Wen-Yi Da, Mao-Lei Yu, Wen-Bin Yang, Meng-Yuan Zhu, Hai Xu et al. "Thermal Stratification and Its Impacts on Water Quality in Shahe Reservoir, Liyang, China." *Huan Jing ke Xue= Huanjing Kexue* 39, no. 6 (2018): 2632-2640.

[2] Rosen, Marc A. "The exergy of stratified thermal energy storages." *Solar energy* 71, no. 3 (2001): 173-185. https://doi.org/10.1016/S0038-092X(01)00036-6

[3] Cabeza, Luisa F. "Advances in thermal energy storage systems: Methods and applications." In *Advances in thermal energy storage systems*, pp. 37-54. Woodhead publishing, 2021. https://doi.org/10.1016/B978-0-12-819885-8.00002-4

[4] Murali, G., and K. Mayilsamy. "Effect of Latent Thermal Energy storage and inlet locations on enhancement of stratification in a solar water heater under discharging mode." *Applied Thermal Engineering* 106 (2016): 354-360. https://doi.org/10.1016/j.applthermaleng.2016.06.030

[5] Hayat, Tasawar, Muhammad Ijaz Khan, Muhammad Farooq, Ahmed Alsaedi, and Muhammad Imran Khan. "Thermally stratified stretching flow with Cattaneo–Christov heat flux." *International Journal of Heat and Mass Transfer* 106 (2017): 289-294. https://doi.org/10.1016/j.ijheatmasstransfer.2016.10.071

[6] Nadeem, S., and Noor Muhammad. "Impact of stratification and Cattaneo-Christov heat flux in the flow saturated with porous medium." *Journal of Molecular Liquids* 224 (2016): 423-430. https://doi.org/10.1016/j.molliq.2016.10.006

[7] Panjwani, Balram, and Jan Erik Olsen. "Design and modelling of dust capturing system in thermally stratified flowing conditions." *Building and Environment* 171 (2020): 106607. https://doi.org/10.1016/j.buildenv.2019.106607

[8] Hayat, T., M. Ijaz Khan, M. Farooq, A. Alsaedi, M. Waqas, and Tabassam Yasmeen. "Impact of Cattaneo–Christov heat flux model in flow of variable thermal conductivity fluid over a variable thicked surface." *International journal of heat and mass transfer* 99 (2016): 702-710. https://doi.org/10.1016/j.ijheatmasstransfer.2016.04.016

[9] Tlili, Iskander, Sania Naseer, Muhammad Ramzan, Seifedine Kadry, and Yunyoung Nam. "Effects of chemical species and nonlinear thermal radiation with 3D Maxwell nanofluid flow with double stratification—an analytical solution." *Entropy* 22, no. 4 (2020): 453. https://doi.org/10.3390/e22040453

[10] Ayet, Alex, and G. G. Katul. "Scaling laws for the length scale of energy-containing eddies in a sheared and thermally stratified atmospheric surface layer." *Geophysical Research Letters* 47, no. 23 (2020): e2020GL089997. https://doi.org/10.1029/2020GL089997

[11] Daniel, Yahaya Shagaiya, Zainal Abdul Aziz, Zuhaila Ismail, and Arifah Bahar. "Unsteady EMHD dual stratified flow of nanofluid with slips impacts." *Alexandria Engineering Journal* 59, no. 1 (2020): 177-189. https://doi.org/10.1016/j.aej.2019.12.020

[12] Ramzan, Muhammad, Naila Shaheen, Seifedine Kadry, Yeu Ratha, and Yunyoung Nam. "Thermally stratified Darcy Forchheimer flow on a moving thin needle with homogeneous heterogeneous reactions and non-uniform heat source/sink." *Applied Sciences* 10, no. 2 (2020): 432. https://doi.org/10.3390/app10020432

[13] Kuznetsov, A. V., and D. A. Nield. "The Cheng–Minkowycz problem for natural convective boundary layer flow in a porous medium saturated by a nanofluid: a revised model." *International Journal of Heat and Mass Transfer* 65 (2013): 682-685. https://doi.org/10.1016/j.ijheatmasstransfer.2013.06.054

[14] Salahuddin, T., Nazim Siddique, Mair Khan, Basem Al Alwan, and Mohammed Almesfer. "Outlining the influence of thermal and solutal stratifications on mixed convection second grade fluid flow near an irregular cylinder with induced magnetic field." *Waves in Random and Complex Media* 34, no. 6 (2024): 5513-5534. https://doi.org/10.1080/17455030.2021.2009153

[15] Ramzan, Muhammad, Mutaz Mohammad, and Fares Howari. "Magnetized suspended carbon nanotubes based nanofluid flow with bio-convection and entropy generation past a vertical cone." *Scientific reports* 9, no. 1 (2019): 12225. https://doi.org/10.1038/s41598-019-48645-9

[16] Ebenezer Olubunmi, Ige, Oyelami Funmilayo Helen, Adedipe Emmanuel Segun, Tlili Iskander, Khan M Ijaz, Khan Sami Ullah, Malik MY, and Xia Wei-Feng. "Analytical simulation of nanoparticle-embedded blood flow control with magnetic field influence through spectra homotopy analysis method." *International Journal of Modern Physics B*.

[17] Mukhopadhyay, Swati, and Anuar Ishak. "Mixed convection flow along a stretching cylinder in a thermally stratified medium." *Journal of Applied Mathematics* 2012, no. 1 (2012): 491695. https://doi.org/10.1155/2012/491695

[18] Ijaz, M., and M. Ayub. "Thermally stratified flow of Jeffrey fluid with homogeneous-heterogeneous reactions and non-Fourier heat flux model." *Heliyon* 5, no. 8 (2019). https://doi.org/10.1016/j.heliyon.2019.e02303

[19] Waqas, M., S. A. Shehzad, T. Hayat, M. Ijaz Khan, and A. Alsaedi. "Simulation of magnetohydrodynamics and radiative heat transport in convectively heated stratified flow of Jeffrey nanofluid." *Journal of Physics and Chemistry of Solids* 133 (2019): 45-51. https://doi.org/10.1016/j.jpcs.2019.03.031

[20] Khashi'ie, Najiyah Safwa, Norihan Md Arifin, Ezad Hafidz Hafidzuddin, and Nadihah Wahi. "Thermally stratified flow of Cu-Al2O3/water hybrid nanofluid past a permeable stretching/shrinking circular cylinder." *Journal of advanced research in fluid mechanics and thermal sciences* 63, no. 1 (2019): 154-163.

[21] Mir, Nazir A., M. Farooq, M. Rizwan, F. Ahmad, S. Ahmad, and B. Ahmad. "Analysis of thermally stratified flow of Sutterby nanofluid with zero mass flux condition." *Journal of Materials Research and Technology* 9, no. 2 (2020): 1631-1639. https://doi.org/10.1016/j.jmrt.2019.11.088

[22] Hayat, Tasawar, Ikram Ullah, Ahmed Alsaedi, and Bashir Ahmad. "Variable aspects of double stratified MHD flow of second grade nanoliquid with heat generation/absorption: a revised model." *Radiation Physics and Chemistry* 157 (2019): 109-115. https://doi.org/10.1016/j.radphyschem.2018.12.021

[23] Khan, Yasir, Qingbiao Wu, Naeem Faraz, and Ahmet Yildirim. "The effects of variable viscosity and thermal conductivity on a thin film flow over a shrinking/stretching sheet." *Computers & Mathematics with Applications* 61, no. 11 (2011): 3391-3399. https://doi.org/10.1016/j.camwa.2011.04.053

[24] Animasaun, I. L. "Effects of thermophoresis, variable viscosity and thermal conductivity on free convective heat and mass transfer of non-darcian MHD dissipative Casson fluid flow with suction and nth order of chemical reaction." *Journal of the Nigerian Mathematical Society* 34, no. 1 (2015): 11-31.

[25] Salawu, S. O., and M. S. Dada. "Radiative heat transfer of variable viscosity and thermal conductivity effects on inclined magnetic field with dissipation in a non-Darcy medium." *Journal of the Nigerian mathematical Society* 35, no. 1 (2016): 93-106. https://doi.org/10.1016/j.jnnms.2015.12.001

[26] Gbadeyan, J. A., E. O. Titiloye, and A. T. Adeosun. "Effect of variable thermal conductivity and viscosity on Casson nanofluid flow with convective heating and velocity slip." *Heliyon* 6, no. 1 (2020). https://doi.org/10.1016/j.heliyon.2019.e03076

[27] Madani Tonekaboni, Seyed Ali, Ramin Abkar, and Reza Khoeilar. "On the Study of Viscoelastic Walters' B Fluid in Boundary Layer Flows." *Mathematical Problems in Engineering* 2012, no. 1 (2012): 861508. https://doi.org/10.1155/2012/861508

[28] Mishra, S. R., S. Baag, and M. M. Bhatti. "Study of heat and mass transfer on MHD Walters B' nanofluid flow induced by a stretching porous surface." *Alexandria engineering journal* 57, no. 4 (2018): 2435-2443. https://doi.org/10.1016/j.aej.2017.08.007

[29] Hayat, T., Sadia Asad, M. Mustafa, and Hamed H. Alsulami. "Heat transfer analysis in the flow of Walters' B fluid with a convective boundary condition." *Chinese Physics B* 23, no. 8 (2014): 084701. https://doi.org/10.1088/1674-1056/23/8/084701

[30] Oyelami, Funmilayo H., Ebenezer O. Ige, Olaide Y. Saka-Balogun, and Oluwaseyi A. Adeyemo. "Study of heat and mass transfer to magnetohydrodynamic (MHD) pulsatile couple stress fluid between two parallel porous plates." *Instrumentation Mesure Métrologie* 20, no. 4 (2021): 179-185. https://doi.org/10.18280/i2m.200401

[31] Jafar, Ahmad Banji, Sharidan Shafie, and Imran Ullah. "Magnetohydrodynamic boundary layer flow of a viscoelastic fluid past a nonlinear stretching sheet in the presence of viscous dissipation effect." *Coatings* 9, no. 8 (2019): 490. https://doi.org/10.3390/coatings9080490

[32] Naganthran, Kohilavani, Md Faisal Md Basir, Thirupathi Thumma, Ebenezer Olubunmi Ige, Roslinda Nazar, and Iskander Tlili. "Scaling group analysis of bioconvective micropolar fluid flow and heat transfer in a porous medium." *Journal of Thermal Analysis and Calorimetry* 143 (2021): 1943-1955. https://doi.org/10.1007/s10973-020-09733-5

[33] Hayat, Tasawar, Muhammad Shoaib Anwar, Muhammad Farooq, and Ahmad Alsaedi. "Mixed convection flow of viscoelastic fluid by a stretching cylinder with heat transfer." *Plos one* 10, no. 3 (2015): e0118815. https://doi.org/10.1371/journal.pone.0118815

[34] Pandya, N., and A. K. Shukla. "Effect of radiation and chemical reaction on an unsteady Walter'sB viscoelastic MHD flow past a vertical porous plate." *Int. J. Adv. Appl. Math. and Mech* 3, no. 3 (2016): 19-26.

[35] Rashed, Gamal M. Abdel-Rahman, and Faiza MN El-fayez. "Studying Radiation and Reaction Effects on Unsteady MHD Non-Newtonian (Walter's B) Fluid in Porous Medium." In *Abstract and Applied Analysis*, vol. 2016, no. 1, p. 9262518. Hindawi Publishing Corporation, 2016. https://doi.org/10.1155/2016/9262518

[36] Tamoor, M., M. Waqas, M. Ijaz Khan, Ahmed Alsaedi, and T. Hayat. "Magnetohydrodynamic flow of Casson fluid over a stretching cylinder." *Results in physics* 7 (2017): 498-502. https://doi.org/10.1016/j.rinp.2017.01.005

[37] Qawasmeh, Bashar R., Mohammad Alrbai, and Sameer Al-Dahidi. "Forced convection heat transfer of Casson fluid in non-Darcy porous media." *Advances in Mechanical Engineering* 11, no. 1 (2019): 1687814018819906. https://doi.org/10.1177/1687814018819906

[38] Sulochana, C., G. P. Ashwinkumar, and N. Sandeep. "Similarity solution of 3D Casson nanofluid flow over a stretching sheet with convective boundary conditions." *Journal of the Nigerian Mathematical Society* 35, no. 1 (2016): 128-141. https://doi.org/10.1016/j.jnnms.2016.01.001

[39] Raju, C. S. K., N. Sandeep, V. Sugunamma, M. Jayachandra Babu, and JV Ramana Reddy. "Heat and mass transfer in magnetohydrodynamic Casson fluid over an exponentially permeable stretching surface." *Engineering Science and Technology, an International Journal* 19, no. 1 (2016): 45-52. https://doi.org/10.1016/j.jestch.2015.05.010

[40] Das, M., R. Mahato, and R. Nandkeolyar. "Newtonian heating effect on unsteady hydromagnetic Casson fluid flow past a flat plate with heat and mass transfer." *Alexandria Engineering Journal* 54, no. 4 (2015): 871-879. https://doi.org/10.1016/j.aej.2015.07.007

[41] Sandeep, N., and C. Sulochana. "Dual solutions for unsteady mixed convection flow of MHD micropolar fluid over a stretching/shrinking sheet with non-uniform heat source/sink." *Engineering Science and Technology, an International Journal* 18, no. 4 (2015): 738-745. https://doi.org/10.1016/j.jestch.2015.05.006

[42] Zheng, Liancun, Jiajia Niu, Xinxin Zhang, and Yingtao Gao. "MHD flow and heat transfer over a porous shrinking surface with velocity slip and temperature jump." *Mathematical and Computer Modelling* 56, no. 5-6 (2012): 133-144. https://doi.org/10.1016/j.mcm.2011.11.080

[43] Mabood, Fazle, and Kalidas Das. "Outlining the impact of melting on MHD Casson fluid flow past a stretching sheet in a porous medium with radiation." *Heliyon* 5, no. 2 (2019). https://doi.org/10.1016/j.heliyon.2019.e01216

[44] Krishnamurthy, M. R., B. C. Prasannakumara, B. J. Gireesha, and Rama Subba Reddy Gorla. "Effect of chemical reaction on MHD boundary layer flow and melting heat transfer of Williamson nanofluid in porous medium." *Engineering Science and Technology, an International Journal* 19, no. 1 (2016): 53-61. https://doi.org/10.1016/j.jestch.2015.06.010

[45] Lund, Liaquat Ali, Zurni Omar, and Ilyas Khan. "Analysis of dual solution for MHD flow of Williamson fluid with slippage." *Heliyon* 5, no. 3 (2019). https://doi.org/10.1016/j.heliyon.2019.e01345

[46] Salawu, S. O., and M. S. Dada. "Radiative heat transfer of variable viscosity and thermal conductivity effects on inclined magnetic field with dissipation in a non-Darcy medium." *Journal of the Nigerian mathematical Society* 35, no. 1 (2016): 93-106. https://doi.org/10.1016/j.jnnms.2015.12.001

[47] Al-Obaidi, Ahmed Ramadhan. "Characterization of internal thermohydraulic flow and heat transfer improvement in a three-dimensional circular corrugated tube surfaces based on numerical simulation and design of experiment." *Heat Transfer* 51, no. 5 (2022): 4688-4713. https://doi.org/10.1002/htj.22519

[48] Al-Obaidi, Ahmed Ramadhan. "Thermal flow and heat performance analyses in circular pipe using different twisted tape parameters based on design of experiments." *Heat Transfer* 51, no. 8 (2022): 7202-7232. https://doi.org/10.1002/htj.22641

[49] Alhamid, Jassim, Ahmed Ramadhan Al-Obaidi, and H. Towsyfyan. "A numerical study to investigate the effect of turbulators on thermal flow and heat performance of a 3D pipe." *Heat Transfer* 51, no. 3 (2022): 2458-2475. https://doi.org/10.1002/htj.22407

[50] Al-Obaidi, Ahmed Ramadhan. "Investigation on effects of varying geometrical configurations on thermal hydraulics flow in a 3D corrugated pipe." *International Journal of Thermal Sciences* 171 (2022): 107237. https://doi.org/10.1016/j.ijthermalsci.2021.107237

[51] Al-Obaidi, Ahmed Ramadhan, and Jassim Alhamid. "Investigation of flow pattern, thermohydraulic performance and heat transfer improvement in 3D corrugated circular pipe under varying structure configuration parameters with development different correlations." *International Communications in Heat and Mass Transfer* 126 (2021): 105394. https://doi.org/10.1016/j.icheatmasstransfer.2021.105394

[52] Al-Obaidi, Ahmed Ramadhan, and Jassim Alhamid. "The effect of different twisted tape inserts configurations on fluid flow characteristics, pressure drop, thermo-hydraulic performance and heat transfer enhancement in the 3D circular tube." *International Journal of Ambient Energy* 44, no. 1 (2023): 57-72. https://doi.org/10.1080/01430750.2022.2091023

[53] Al-Obaidi, Ahmed Ramadhan, Jassim Alhamid, and Faik Hamad. "Flow felid and heat transfer enhancement investigations by using a combination of corrugated tubes with a twisted tape within 3D circular tube based on different dimple configurations." *Heat Transfer* 50, no. 7 (2021): 6868-6885. https://doi.org/10.1002/htj.22207

[54] Fagbade, A. I., B. O. Falodun, and A. J. Omowaye. "MHD natural convection flow of viscoelastic fluid over an accelerating permeable surface with thermal radiation and heat source or sink: spectral homotopy analysis approach." *Ain Shams Engineering Journal* 9, no. 4 (2018): 1029-1041. https://doi.org/10.1016/j.asej.2016.04.021

[55] Idowu, Amos Sesan, and B. O. Falodun. "Variable thermal conductivity and viscosity effects on non-Newtonian fluids flow through a vertical porous plate under Soret-Dufour influence." *Mathematics and Computers in Simulation* 177 (2020): 358-384. https://doi.org/10.1016/j.matcom.2020.05.001

[56] Mehmood, Ahmer, Asif Ali, and Tariq Shah. "Heat transfer analysis of unsteady boundary layer flow by homotopy analysis method." *Communications in Nonlinear Science and Numerical Simulation* 13, no. 5 (2008): 902-912. https://doi.org/10.1016/j.cnsns.2006.09.008

[57] Walters, K. J. "Non-Newtonian effects in some elastico-viscous liquids whose behaviour at small rates of shear is characterized by a general linear equation of state." *The Quarterly Journal of Mechanics and Applied Mathematics* 15, no. 1 (1962): 63-76. https://doi.org/10.1093/qjmam/15.1.63

[58] Alao, F. I., A. I. Fagbade, and B. O. Falodun. "Effects of thermal radiation, Soret and Dufour on an unsteady heat and mass transfer flow of a chemically reacting fluid past a semi-infinite vertical plate with viscous dissipation." *Journal of the Nigerian mathematical Society* 35, no. 1 (2016): 142-158. https://doi.org/10.1016/j.jnnms.2016.01.002

[59] Motsa, S. S. "New iterative methods for solving nonlinear boundary value problems." In *Fifth Annual Workshop on Computational Applied Mathematics and Mathematical Modeling in Fluid Flow*, pp. 9-13. Pietermaritzburg Campus: School of Mathematics, Statistics and Computer Science, 2012.

[60] Liao, Shi-Jun. "The proposed homotopy analysis technique for the solution of nonlinear problems." PhD diss., Ph. D. Thesis, Shanghai Jiao Tong University, 1992.

[61] Hussaini, M. Yousuff, and Thomas A. Zang. *Spectral methods in fluid dynamics*. No. NAS 1.26: 178103. 1986.

[62] Memon, Abid Ali, Muhammad Asif Memon, Kaleemullah Bhatti, and Gul Muhammad Shaikh. "Finite element simulation of Newtonian and non-Newtonian fluid through the parallel plates affixed with single screen." *European Journal of Pure and Applied Mathematics* 13, no. 1 (2020): 69-83. https://doi.org/10.29020/nybg.ejpam.v13i1.3586

[63] Ayub, Assad, Tanveer Sajid, Wasim Jamshed, William Rolando Miranda Zamora, Leandro Alonso Vallejos More, Luz Marina Galván Talledo, Nélida Isabel Rodríguez Ortega de Peña, Syed M. Hussain, Muhammad Bilal Hafeez, and Marek Krawczuk. "Activation energy and inclination magnetic dipole influences on Carreau nanofluid flowing via cylindrical channel with an infinite shearing rate." *Applied Sciences* 12, no. 17 (2022): 8779. https://doi.org/10.3390/app12178779

[64] Jahan, Shah, Hamzah Sakidin, Roslinda Nazar, and Ioan Pop. "Analysis of heat transfer in nanofluid past a convectively heated permeable stretching/shrinking sheet with regression and stability analyses." *Results in Physics* 10 (2018): 395-405. https://doi.org/10.1016/j.rinp.2018.06.021